Received 23 December 2021; revised 31 January 2022; accepted 21 February 2022. Date of publication 1 March 2022; date of current version 15 March 2022.

Digital Object Identifier 10.1109/OJCOMS.2022.3155648

Molecule Harvesting Transmitter Model for Molecular Communication Systems

ARMAN AHMADZADEH [1], VAHID JAMALI [2] (Member, IEEE), AND ROBERT SCHOBER [1] (Fellow, IEEE)

[1]Institute for Digital Communication, University of Erlangen–Nuremberg, 91054 Erlangen, Germany

[2]Department of Electrical and Computer Engineering, Princeton University, Princeton, NJ 08544, USA

CORRESPONDING AUTHOR: A. AHMADZADEH (e-mail: arman.ahmadzadeh@fau.de)

This work was supported in part by the German Science Foundation (DFG) under Grant SCHO 831/9-1, and in part by the German Federal Ministry of Education and Research (BMBF) under Grant MAMOKO 16KIS0913.

ABSTRACT This paper develops mathematical models for molecule harvesting transmitters in diffusive molecular communication (MC) systems. In particular, we consider a communication link consisting of a spherical transmitter nano-machine and a spherical receiver nano-machine suspended in a fluid environment. The transmitter and the receiver exchange information via signaling molecules. The transmitter is equipped with molecule harvesting units on its surface. Signaling molecules which come into contact with the harvesting units may be re-captured by the transmitter. For this system, we derive closed-form expressions for the channel impulse response and harvesting impulse response. Furthermore, we extend the harvesting transmitter model to the case of continuous signaling molecule release. In particular, we derive closed-form expressions for the average received signal at the receiver and the average harvested signal at the transmitter for different temporal release rates namely, constant, linearly increasing, and linearly decreasing release rates. Finally, we validate the accuracy of the derived mathematical expressions via particle-based simulations.

INDEX TERMS Transmitter modeling, molecule harvesting, energy harvesting transmitter, diffusive molecular communication.

I. INTRODUCTION

MOLECULAR communication (MC) enables synthetic communication at nano-scale. In MC systems, molecules are exploited as carriers of information for the exchange of messages between transmitter and receiver nano-machines [1]–[3]. Examples of MC systems are abundant in nature. This includes, among many others, the communication between cells via signaling molecules and quorum sensing of bacteria via autoinducers. MC systems may find application in health monitoring, nano-medicine, environmental and industrial monitoring, see, e.g., [1], [2].

Communication systems can be designed and optimized with respect to several key performance indicators (KPIs) such as reliability, energy efficiency, latency, etc. However, independent of the KPI adopted, the mathematical modeling of the components of the communication system, i.e., the transmitter, the channel, and the receiver plays a crucial role for design and optimization [4]. Without meaningful component models, design and optimization are very cumbersome and heuristic approaches must be adopted. Hence, developing mathematical component models is an important first step for system design. In diffusive MC systems, the transmitter nano-machine releases signaling molecules into a fluid environment, where the released molecules are transported via *passive diffusion*, without consuming extra energy. The transport of the signaling molecules can also be affected by external factors such as *flow* and *chemical reaction networks*. In particular, the impact of flow on the performance can be constructive or destructive depending on the direction, magnitude, and randomness of the flow. Furthermore, signaling molecules entering the channel can be consumed by chemical reaction networks and degraded, such that they do not reach the receiver nano-machine. Signaling molecules that do reach the receiver nano-machine can potentially be observed and exploited for decoding the conveyed message [4].

The transmitter nano-machine can mitigate to some extent the disruptive effects of the impairments introduced by the channel. For instance, one approach to mitigate the impact of

degradation reactions and/or flow in an undesired direction is for the transmitter nano-machine to control the release of the signaling molecules by increasing the number of released molecules and prolonging the release duration. On the other hand, the production of signaling molecules is an energy consuming process in general. For instance, in nature, cells produce signaling molecules by consuming adenosine triphosphate (ATP), see [5]. As a result, although releasing more signaling molecules seems promising, this comes at the expense of a higher energy consumption. In nature, there are also other mechanisms for increasing the number of available signaling molecules. One relevant approach employed by neurons is via harvesting previously released signaling molecules. In particular, neurons are equipped with re-uptake units, e.g., dopamine transporters, responsible for harvesting of signaling (dopamine) molecules, see [6]. Thus, developing meaningful models for transmitters that can harvest signaling molecules is of particular importance for the design of synthetic MC systems and is the focus of this paper.

Transmitter modeling at nano-scale involves several different aspects. Aspect 1) concerns the temporal release pattern of the signaling molecules, e.g., 1-a) instantaneous or 1-b) continuous release. Aspect 2) concerns the physical and chemical properties of the transmitter; including 2-a) the chemical reaction networks responsible for the production of signaling molecules, 2-b) the mechanisms responsible for the internal transportation of the produced molecules to the transmitter surface, and 2-c) the mechanisms controlling the release of the signaling molecules into the channel. In the MC literature, the majority of works adopt a *point* transmitter model with instantaneous release, see, e.g., [7]–[11]. In [12], the impact of 2-a) for a point transmitter with limited signaling molecule storage capacity and adaptive continuous release is considered. In [13], a point transmitter model taking 1-b) into account is proposed, where exponential and rectangular temporal release patterns are investigated. In [14], a volume transmitter model is considered, where molecules are initially uniformly distributed inside the volume of the transmitter and instantaneously released. Furthermore, it is assumed that the surface of the transmitter is transparent and does not impede the diffusion of signaling molecules. The authors of [14] and [15] further relax the assumption of a transparent transmitter surface and numerically investigate volume transmitter models with fully *reflective* surfaces. In [16], ion-channel-based transmitter models are developed with the main focus on aspect 2-c). Ion-channel-based transmitters are equipped with ion-channel gates embedded in the transmitter membrane for controlling the release of signaling molecules. The opening and closing of the gates are controlled by a so-called gating parameter such as a voltage or a ligand. The model proposed in [16] does not consider the impact of 2-a) and assumes passive diffusion for the transportation of the particles inside the transmitter. In [17]–[19], transmitter models taking into account jointly aspects 2-a) and 2-b) are developed. There, mesoscopic models are employed and the corresponding reaction-diffusion equation is *numerically* solved to capture the joint impact of 2-a) and 2-b). In the most recent work, the authors of [20] proposed membrane fusions-based (FB) transmitter models with the main focus on aspects 2-b) and 2-c). In particular, in [20], it is assumed that signaling molecules are encapsulated in vesicles, where the transportation of the vesicles inside the transmitter is modeled via passive diffusion. The molecules are released by fusion of the vesicles with the transmitter membrane, which is modeled via a chemical reaction. We note that none of the works mentioned above, i.e., [14]–[20], takes signaling molecule harvesting into account. High-level discussions of molecule harvesting mechanisms in the context of MC systems are presented in [21]. In [22], the concept of molecule harvesting is employed at the relay node of a two-hop relay network, where a *deterministic* chemical reaction model is used for describing the molecule harvesting mechanism. In [23], the problem of molecule harvesting in the context of neurons is investigated. The harvesting process (referred to as re-uptake in [23]) is modeled via *Stochastic* chemical reactions. There, the joint effects of diffusion, degradation in the channel, and spill over are taken into account. In [23], the geometry of the transmitter and receiver are modeled as finite plains motivated by the geometry of neurons, and the instantaneous release of signaling molecules is assumed.

To the best of the authors' knowledge, this paper is the first work that accounts for the joint effects of 1-b) continuous release, degradation in the channel, and the 2-c) controlled release together with the harvesting of signaling molecules at the transmitter. Furthermore, we illustrate some of the benefits of molecule harvesting (MH) transmitters, which include 1) inter-symbol-interference (ISI) reduction, 2) the possibility of performing transmitter-side channel state information (CSI) acquisition, and 3) molecule harvesting (recycling) for future transmissions. In particular, we make the following contributions.

- We derive mathematical closed-form expressions for the channel impulse response and the harvesting impulse response. The channel impulse response (harvesting impulse response) represents the probability of observing (harvesting) a single molecule after its release from the surface of the transmitter at the receiver (transmitter), while taking degradation in the channel and absorption on the transmitter surface into account.
- We conduct a dimensional analysis and present the partial differential equations describing the channel and harvesting impulse responses in dimensionless form. The dimensional analysis generalizes our system model and reduces the number of variables that appear in the relevant expressions.
- Equipped with the expressions for the channel and harvesting impulse responses, we derive closed-form expressions for the *average* received signal at the receiver and the *average* harvested signal at the transmitter, respectively, for continuous release of signaling molecules by the transmitter nano-machine while taking aspect 2-c) into account. Here, three different temporal

release rates namely, constant, linearly increasing, and linearly decreasing release rates are studied.
- We assess the accuracy of the derived mathematical expressions with particle-based simulations and provide insight for system design.

The rest of this paper is organized as follows. In Section II, we introduce the system model. In Section III, we derive closed-form analytical expressions for the channel and harvesting impulse responses and perform a dimensional analysis. Then, in Section IV, we exploit the channel and harvesting impulse responses to derive analytical expressions for the expected received signal and the expected harvested signal, respectively. In Section V, we present simulation and analytical results, and, finally, the conclusions of the paper are drawn in Section VI.

II. SYSTEM MODEL

In this section, we describe the system model considered in this paper. An unbounded three-dimensional fluid environment with constant temperature and constant viscosity is considered. The receiver is modeled as a passive sphere[1] with radius $a_{\rm rx}$. We assume that the center of the receiver is located at $\vec{r}_{\rm rx} = (x_{\rm rx}, y_{\rm rx}, z_{\rm rx})$ in a three dimensional Cartesian coordinate system. The transmitter is modeled as a *hard sphere* (i.e., reactive with signaling molecules) with radius $a_{\rm tx}$ and the center located in the origin of the coordinate system, i.e., $\vec{r}_{\rm tx} = (x_{\rm tx}, y_{\rm tx}, z_{\rm tx}) = (0, 0, 0)$. The transmitter uses a specific type of molecule, denoted by type A and referred to as information or signaling molecule, for communication with the receiver. The surface of the transmitter is covered by components that control the release of the signaling molecules and are referred to as release units. Furthermore, we assume that each release unit has two states, namely, an open state and a closed state. When the release units are open, signaling molecules are released from the surface of the transmitter with a rate of $\mu(t)$ [molecule/s]. On the other hand, when the release units are closed, no signaling molecule is released from the surface of the transmitter, see Fig. 1. Ion-channels embedded in the membrane of cells are one example of release units in nature, where the opening and closing is mediated by a *gate parameter*, e.g., a voltage or ions [5]. In this work, we model the external stimulus (e.g., gate parameter in ion-channels) controlling the opening and the closing of the release units only implicitly. In other words, we assume that there is a one-to-one mapping between the presence (absence) of the stimulus and the opening (closing) of the release unit. We refer the interested reader to [16] for a detailed discussion of ion-channel transmitter models. Moreover, we assume that the release units,

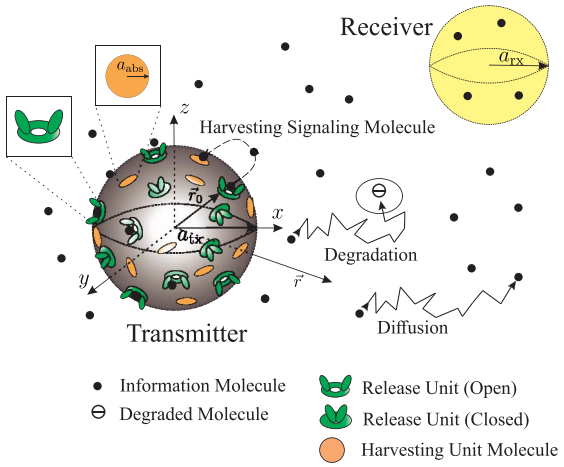

FIGURE 1. Schematic diagram of the considered system. Transmitter and receiver are shown as a gray sphere in the center of the coordinate system and a yellow sphere, respectively. The surface of the transmitter is partially covered with harvesting unit molecules of type *B*, shown in orange color, where each harvesting unit is modeled as a circular patch with radius $a_{\rm abs}$. One sample trajectory of an *A* molecule that is harvested (or absorbed) by a *B* molecule is depicted by a dashed arrow. The release units on the surface of the transmitter are shown in green color, and can assume two different states, i.e., the open state and the closed state. Two sample trajectories of an *A* information molecule (denoted by a black dot) that result in a degraded molecule (circle with a "−" inside) and a displacement via diffusion are illustrated by solid arrows.

$U_i, i \in \{1, 2, \ldots, U_{\max}\}$, are uniformly distributed across the surface of the transmitter. In the remainder of this paper, we denote the symbol duration by $T_{\rm sym}$ [s]. We further assume that $T_{\rm sym}$ is split into two parts namely, $T_{\rm on}$ and $T_{\rm off}$. During $T_{\rm on}$ an external stimulus is applied ($T_{\rm on} \leq T_{\rm sym}$ [s]), such that A molecules are discharged from the release units with rate $\mu(t)$ [molecule/s], while all release units are closed for a duration of $T_{\rm off} = T_{\rm sym} - T_{\rm on}$ [s], see Fig. 2.

In addition to the release units, we assume that the transmitter is equipped with a component that is able to harvest signaling molecules. We refer to this component as harvesting unit.[2] One example of harvesting units in nature are neurotransmitter transporters embedded in the membrane of pre-synaptic neurons and responsible for re-uptake of previously released neurotransmitters such as dopamine and serotonin. Another example for such a mechanism is receptor internalization in autocrine signaling, see [26] and references therein. In nature, autocrine signaling is the process of binding the signaling molecule of a cell to the cell's own receptors [5]. Autocrine signaling regulates many physiological cell processes, for instance, it helps cells to reinforce their correct identities during their growth and division. Moreover, it also plays an important role during the homeostatic process

1. In this work, in order to keep the analysis mathematically tractable, we assume a transparent receiver model. However, we note that transparent receiver models are good candidates for modeling passive measurement devices, such as pH sensors, see, e.g., [24]. Furthermore, the extension of the results reported in this work to other receiver models, such as absorbing receivers and reactive receivers, is an interesting direction for future research.

2. Molecule harvesting units can be realized and integrated into practical MC transmitters, see, e.g., [25]. Examples of biological building blocks that can potentially realize the functionalities of a molecule harvesting unit include: a) light-driven inward proton pumps, capable of transporting protons (signaling molecules) from the surrounding medium into the interior of the transmitter, b) adenosine triphosphate (ATP)-driven and light-driven active calcium ion transporters, capable of harvesting calcium ions (signaling molecules), c) dopamine transporters capable of harvesting dopamine neurotransmitters in the synaptic cleft. In fact, the integration of such molecule harvesting units in future practical MC transmitters and their experimental demonstration are interesting research directions.

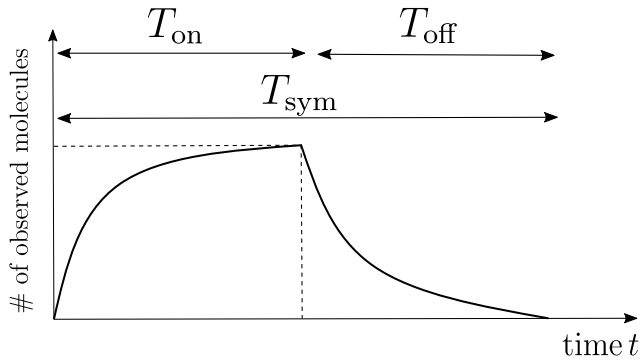

FIGURE 2. A sample received signal in terms of the number of molecules observed at the receiver. During the T_{on} period, A molecules are released from the surface of the transmitter with rate $\mu(t)$, and some of them may reach the receiver. During the T_{off} period, no molecules are released, i.e., $\mu(t) = 0$. $T_{\text{sym}} = T_{\text{on}} + T_{\text{off}}$.

which characterizes the macrophages of the immune system. Receptor internalization is a step in which the ligand-receptor complex is transported inside the cell leading to the dissociation of the binding ligand, see [26] for a detailed discussion of autocrine signaling and receptor internalization modeling. For the sake of the mathematical tractability of our analysis, here, we model the interaction of the signaling molecules with the harvesting units as a second-order irreversible bi-molecular reaction given as follows

$$A + B \xrightarrow{k_{\text{abs}}} A + E, \tag{1}$$

where B represents the harvesting unit molecule, E denotes any potential product molecule other than the signaling molecule, and k_{abs} is the harvesting or absorbing microscopic reaction rate constant in [molecule^{-1}m^{3}s^{-1}]. Eq. (1) is also used in [23] for modeling the re-uptake process in neurons and in [26] for modeling receptor internalization. In this work, we model the harvesting unit molecules as circular patches with radius a_{abs}, and assume that they are uniformly distributed across the surface of the transmitter.

Information molecules discharged from the release units perform a random walk in the environment in all directions and some of them may reach the receiver. Thereby, we assume that the diffusion processes of different signaling molecules are mutually independent. We denote the diffusion coefficient of information molecule A by D_A. Furthermore, we assume that A molecules performing the random walk can be uniformly degraded in the entire environment (or channel) via a reaction mechanism of the form

$$A \xrightarrow{k_{\text{d}}} \emptyset, \tag{2}$$

where k_{d} is the degradation reaction constant in [s^{-1}] and $\emptyset$ is a species of molecules which is not recognized by the receiver. Eq. (2) models a first-order reaction but can also be used to approximate higher order reactions, see, e.g., [27]–[29].

III. CHANNEL AND HARVESTING IMPULSE RESPONSES

In this section, we first formulate the problem that needs to be solved for derivation of the channel and harvesting impulse responses. Subsequently, we perform a dimensional analysis and convert the formulated problem into its dimensionless form. Finally, we obtain the Green's function of the system as a key building block for calculation of the channel and harvested impulse responses.

A. DEFINITIONS

Here, we formally define the *channel impulse response* and the *harvesting impulse response* as follows.

Definition 1 (Channel Impulse Response): We define the *channel impulse response* as the probability of *observing* a given A molecule inside the volume of a transparent receiver between time t and $t + \mathrm{d}t$. Here, we assume that the given A molecule was discharged at time t_0 from a release unit, uniformly distributed on the surface of a spherical transmitter and located at a distance $|\vec{r}_0| = r_0 = a_{\text{tx}}$ from the center of the transmitter. Moreover, the released A molecule may undergo either one of the two reactions specified in (1) and (2) during time t. We denote this probability as $P_A(t|r_0)$.

Definition 2 (Harvested Impulse Response): The *harvested impulse response* is defined as the probability of *harvesting* a given A molecule at the transmitter up until time t. Here, we assume that the given A molecule was discharged at time t_0 from a release unit uniformly distributed on the surface of a spherical transmitter and located at a distance $|\vec{r}_0| = r_0 = a_{\text{tx}}$ from the center of the transmitter. Moreover, the released A molecule may undergo either one of the two reactions specified in (1) and (2) during time t. We denote this probability as $P_A^{\text{Harv}}(t|r_0)$.

B. PROBLEM FORMULATION

Let us assume, for the moment, that the *entire* surface of the transmitter is covered with infinitely many harvesting molecules B. In other words, for the moment, we neglect the physical dimension of the harvesting molecules B. This assumption facilitates the derivation of closed-form expressions for $P_A(t|r_0)$ and $P_A^{\text{Harv}}(t|r_0)$. Later, at the end of this section, we relax this idealistic assumption to account for the non-zero dimension and finite number of B molecules. To this end, we will use the technique of "boundary homogenization", see [30] and references therein.

In the following, we first define another probability term, which will be exploited for calculation of both $P_A(t|r_0)$ and $P_A^{\text{Harv}}(t|r_0)$. In particular, the probability that a given A molecule released uniformly at a distance r_0 from the center of the transmitter at time $t_0 = 0$ is at location $[\vec{r}, \vec{r} + \mathrm{d}\vec{r})$ at time $[t, t + \mathrm{d}t)$, given that this molecule may undergo either one of the two reactions introduced in (1) and (2) by the time $[t, t + \mathrm{d}t)$, is denoted by $P_A(\vec{r}, t|r_0)$. Now, let us assume that $P_A(\vec{r}, t|r_0)$ is known. Then, we can evaluate the incoming probability flux,[3] $-J(\vec{r}, t|r_0)$, at the surface of

3. We note that the probability flux refers to the flux of the position probability of a *single* A molecule, whereas the conventional diffusive molecule flux (used in Fick's first law of diffusion) refers to the flux of the average number of A molecules. For further details on probability flux, we refer the interested reader to [31, Ch. 3].

the transmitter by applying Einstein's theory of diffusion as follows [31, eq. (3.34)]

$$-J(\vec{r},t|r_0)\big|_{\vec{r}\in\Omega_{\rm tx}} = D_A\nabla P_A(\vec{r},t|r_0)\big|_{\vec{r}\in\Omega_{\rm tx}}, \tag{3}$$

where ∇ is the gradient operator in spherical coordinates and $\Omega_{\rm tx}$ is the surface of the transmitter. Now, given $-J(\vec{r},t|r_0)$, $-J(\vec{r},t|r_0)\mathrm{d}\Omega_{\rm tx}\mathrm{d}t$ is the probability that a given A molecule reacts with the infinitesimally small surface element $\mathrm{d}\Omega_{\rm tx}$ of the transmitter during infinitesimally small time $\mathrm{d}t$. Integrating this function over time and the surface of the transmitter yields a relation between $P_A^{\rm Harv}(t|r_0)$ and $P_A(\vec{r},t|r_0)$ as follows [31, eq. (3.35)]

$$P_A^{\rm Harv}(t|r_0) = -\int_0^t \oiint_{\Omega{\rm tx}} J(\vec{r},\tau|r_0)\mathrm{d}\Omega_{\rm tx}\mathrm{d}\tau. \tag{4}$$

Moreover, still assuming $P_A(\vec{r},t|r_0)$ is known, integrating $P_A(\vec{r},t|r_0)$ over time and the volume of the receiver yields a relation between $P_A(t|r_0)$ and $P_A(\vec{r},t|r_0)$ as follows

$$P_A(t|r_0) = \oiiint_{v{\rm rx}} P_A(\vec{r},t|r_0)\mathrm{d}\vec{r}, \tag{5}$$

where $v_{\rm rx}$ describes all points in space that are inside the volume of the receiver. Thus, for evaluation of both $P_A(t|r_0)$ and $P_A^{\rm Harv}(t|r_0)$, we first need to determine $P_A(\vec{r},t|r_0)$.

Clearly, the evaluation of (3) requires knowledge of $J(\vec{r},t|r_0)$ only on the surface of the transmitter, i.e., on $\Omega_{\rm tx}$. However, since we assume that both type B molecules and the release units are *uniformly* distributed on the surface of the transmitter, $J(\vec{r},t|r_0)$ and $P_A(\vec{r},t|r_0)$ are only functions of the magnitude of $\vec{r}$, denoted by r, and not of $\vec{r}$ itself. In other words, due to symmetry, $J(\vec{r},t|r_0)$ in (4) is independent of azimuth angle θ and polar angle ϕ and only depends on r. In the remainder of this paper, we substitute $\vec{r}$ with its magnitude r in (3), (4), and (5) without loss of generality. As a result, (3) and (4) can be combined as

$$P_A^{\rm Harv}(t|r_0) = \int_0^t 4\pi a_{\rm tx}^2 D_A \frac{\partial P_A(r,\tau|r_0)}{\partial r}\bigg|_{r=a_{\rm tx}} \mathrm{d}\tau. \tag{6}$$

In the following, we formulate the problem of finding $P_A(r,t|r_0)$ for the system model specified in Section II and for the case where the entire surface of the transmitter is covered by infinitely many zero-dimensional harvesting unit B molecules. To this end, we start with the general form of the reaction-diffusion equation for the degradation reaction in (2), which can be written as follows [32]

$$\frac{\partial P_A(r,t|r_0)}{\partial t} = D_A\nabla^2 P_A(r,t|r_0) - k_{\rm d}P_A(r,t|r_0), \tag{7}$$

where ∇^2 is the Laplace operator in spherical coordinates. Due to the uniform distribution of the release units, the release of a given A molecule at distance r_0 at time $t_0 = 0$ can be modeled by the following initial condition

$$P_A(r,t\to 0|r_0) = \frac{1}{4\pi r_0^2}\delta(r-r_0), \tag{8}$$

where constant $1/(4\pi r_0^2)$ is a normalization factor and $\delta(\cdot)$ is the Dirac delta function. The boundary conditions of the system model for the assumed unbounded environment and the reaction mechanism in (1) on the surface of the transmitter can be written as follows [33, eqs. (3), (4)]

$$\lim_{r\to\infty} P_A(r,t|r_0) = 0, \tag{9}$$

and

$$4\pi a_{\rm tx}^2 D_A \frac{\partial P_A(r,t|r_0)}{\partial r}\bigg|_{r=a_{\rm tx}} = k_{\rm abs}P_A(r\to a_{\rm tx},t|r_0). \tag{10}$$

The solution of reaction-diffusion equation (7) with initial and boundary conditions (8)-(10) is the Green's function[4] of our system model.

To summarize, obtaining $P_A(t|r_0)$ and $P_A^{\rm Harv}(t|r_0)$ requires knowledge of $P_A(r,t|r_0)$ which is the Green's function based on (7).

C. DIMENSIONAL ANALYSIS

In this subsection, in order to simplify our derivations and generalize our results, we provide a dimensional analysis and rewrite our system model and problem formulation in dimensionless form, where we denote the dimensionless variables by superscript "$\prime$". Given the dimensionless variables, the corresponding dimensional variables can be obtained by scaling the dimensionless variables by reference variables.

Let us denote the reference distance in m and the reference number of molecules by $r_{\rm ref}$ and $N_{A\rm ref}$, respectively. Then, we define the dimensionless time as $t' = D_A t/r_{\rm ref}^2$ and the dimensionless radial distance from the center of the transmitter as $r' = r/r_{\rm ref}$. The dimensionless reaction rate constants in (1) and (2) can be written as

$$k'_{\rm abs} = \frac{k_{\rm abs}N_{A\rm ref}}{D_A r_{\rm ref}} \quad \text{and} \quad k'_{\rm d} = \frac{k_{\rm d}r_{\rm ref}^2}{D_A}. \tag{11}$$

For consistency of notation, we also denote $P_A(r,t|r_0)$, $P_A^{\rm Harv}(t|r_0)$, and $P_A(t|r_0)$ for dimensionless variables r', t', and r'_0 as $P'_A(r',t'|r'_0)$, $P'^{\rm Harv}_A(t'|r'_0)$, and $P'_A(t'|r'_0)$, respectively. In the following, without loss of generality, we choose $r_{\rm ref} = a_{\rm tx} = r_0$ and $N_{A\rm ref} = 1$. Thus, in what follows r'_0 can be set to 1. Specifically, (6) in dimensionless form can be written as

$$P'^{\rm Harv}_A(t'|r'_0) = \int_0^{t'} 4\pi \frac{\partial P'_A(r',\tau'|r'_0)}{\partial r'}\bigg|_{r'=1} \mathrm{d}\tau'. \tag{12}$$

Furthermore, reaction-diffusion equation (7) becomes

$$\frac{\partial P'_A(r',t'|r'_0)}{\partial t'} = \nabla^2 P'_A(r',t'|r'_0) - k'_{\rm d}P'_A(r',t'|r'_0), \tag{13}$$

where

$$\begin{aligned}\frac{\partial P'_A(r',t'|r'_0)}{\partial t'} &= \frac{a^2}{D_A}\frac{\partial P_A(r,t|r_0)}{\partial t},\\ \nabla^2 P'_A(r',t'|r'_0) &= a^2\nabla^2 P_A(r,t|r_0).\end{aligned} \tag{14}$$

4. The solution of an inhomogeneous partial differential equation for an initial condition in the form of a Dirac delta function is referred to as the Green's function [34].

Initial condition (8) and the first boundary condition (9) can be written as

$$P_A(r', t' \to 0|r'_0) = \frac{1}{4\pi {r'_0}^2}\delta(r' - r'_0) \tag{15}$$

and

$$\lim_{r' \to \infty} P'_A(r', t'|r'_0) = 0, \tag{16}$$

respectively. The second boundary condition, given in (10), simplifies in dimensionless form to

$$4\pi \frac{\partial P'_A(r', t'|r'_0)}{\partial r'}\bigg|_{r'=1} = k'_{\text{abs}} P_A\big(r' \to 1, t'|r'_0\big). \tag{17}$$

D. GREEN'S FUNCTION

In this subsection, we derive a closed-form analytical expression for the Green's function of the system, $P'_A(r', t'|r'_0)$. To this end, we adopt the methodology introduced in [35]. In particular, we decompose $P'_A(r', t'|r'_0)$ as follows

$$P'_A(r', t'|r'_0) = U'(r', t'|r'_0) + V'\big(r', t'|r'_0\big), \tag{18}$$

where function $U'(r', t'|r'_0)$ is chosen such that it satisfies both the reaction-diffusion equation (13) and initial condition (15). On the other hand, function $V'(r', t'|r'_0)$ is chosen such that it satisfies (13), but at the same time, also satisfies jointly with function $U'(r', t'|r'_0)$ boundary conditions (16) and (17). With this approach, we can decompose the original problem into two sub-problems as follows. In the first sub-problem, we solve the reaction-diffusion equation

$$\frac{\partial U'(r', t'|r'_0)}{\partial t'} = \nabla^2 U'\big(r', t'|r'_0\big) - k'_{\text{d}} U'\big(r', t'|r'_0\big), \tag{19}$$

with initial condition

$$U'(r', t' \to 0|r'_0) = \frac{1}{4\pi {r'_0}^2}\delta(r' - r'_0). \tag{20}$$

In the second sub-problem, we solve the reaction-diffusion equation

$$\frac{\partial V'(r', t'|r'_0)}{\partial t'} = \nabla^2 V'(r', t'|r'_0) - k'_{\text{d}} V'(r', t'|r'_0), \tag{21}$$

with the initial condition

$$V'(r', t' \to 0|r'_0) = 0. \tag{22}$$

Finally, the solutions of both sub-problems are combined, cf. (18), such that they jointly satisfy boundary conditions (9) and (10). The solution for the Green's function is given in the following theorem.

Theorem 1 (Green's Function): The probability of finding a given A molecule at dimensionless time t' at dimensionless distance $r' \geq r'_0$ from the center of the transmitter, given that it was released from a release unit at dimensionless distance $r'_0 = 1$ at dimensionless time ${t_0}' = 0$ and potentially degraded via first-order degradation reaction (2) (with dimensionless reaction constant k'_{d}) and/or harvested by a harvesting unit on the transmitter surface via second-order reaction (1) (with dimensionless harvesting reaction rate constant k'_{abs}) during dimensionless time t', is given as follows

$$P'_A(r', t'|r'_0) = \frac{\exp\big(-k'_{\text{d}} t'\big)}{4\pi r'}\Bigg[\frac{1}{\sqrt{\pi t'}} \times \exp\left(\frac{-\big(r'-1\big)^2}{4t'}\right) - \alpha' \exp\Big(\alpha'\big(r'-1\big) + (\alpha')^2 t'\Big) \times \operatorname{erfc}\left(\frac{r'-1}{\sqrt{4t'}} + \alpha'\sqrt{t'}\right)\Bigg], \tag{23}$$

where $\operatorname{erfc}(\cdot)$ is the complementary error function and constant α' is defined as

$$\alpha' = 1 + \frac{k'_{\text{abs}}}{4\pi} \tag{24}$$

Proof: The proof is provided in Appendix A. ■

Given (23), $P'_A(t'|r'_0)$ and $P'^{\text{Harv}}_A(t'|r'_0)$ are obtained via (5) (in its dimensionless form) and (12), respectively. In particular, $P'_A(t'|r'_0)$ is calculated as

$$P'_A(t'|r'_0) = V_{\text{rx}} P'_A(r'_{\text{rx}}, t'|r'_0), \tag{25}$$

where V_{rx} is the volume of the receiver and we invoked the *uniform concentration assumption*[5] Similarly, $P'^{\text{Harv}}_A(t'|r'_0)$ is obtained as follows

$$P'^{\text{Harv}}_A(t'|r'_0) = \frac{k'_{\text{abs}}}{4\pi}\Bigg[\frac{-\alpha'}{(\alpha')^2 - k'_{\text{d}}} \exp\Big(\big(\alpha'\big)^2 t' - k'_{\text{d}} t'\Big) \times \operatorname{erfc}\big(\alpha'\sqrt{t}\big) + \frac{\sqrt{k'_{\text{d}}}}{(\alpha')^2 - k'_{\text{d}}} \times \operatorname{erfc}\left(\sqrt{k'_{\text{d}} t'}\right) + \frac{1}{\alpha' + \sqrt{k'_{\text{d}}}}\Bigg]. \tag{26}$$

E. PHYSICAL PROPERTIES OF HARVESTING UNITS

So far, we neglected the physical dimension of the B molecules and modeled them as infinitely many zero-dimensional points on the surface of the transmitter. In order to take the size (i.e., circular patches with radius a'_{abs}) and the finite number of the B molecules into account, boundary condition (17) has to be modified to represent only that part of the transmitter surface which is covered by B molecules. However, this makes the derivation of $P'_A(r', t'|r'_0)$ very difficult, if not impossible. One approach to circumvent this difficulty is to use the *boundary homogenization* technique, see [30] and references therein. For boundary homogenization, a non-homogenized surface is substituted with a virtual homogenized surface with properly modified chemical and physical properties. For the problem at hand, the transmitter's surface partially covered with B molecules is substituted with a transmitter whose surface is covered with infinitely many zero-dimensional B molecules (the case that was considered at the beginning of this section) but with a modified

5. The uniform concentration assumption implies that the concentration of the signaling molecules at any point inside the volume of the receiver is equal to that in the center of the receiver [28].

k'_{abs}. We denote this modified absorption rate by $k^{\star}_{\text{abs}}$. It can be shown[6] [30] that $k^{\star}_{\text{abs}}$ is given by

$$k^{\star}_{\text{abs}} = \frac{4\pi k'_{\text{abs}}\varphi'}{k'_{\text{abs}}(1-\varphi')+4\pi},$$
$$\varphi' = \frac{M\left(a'_{\text{abs}}\right)^2\left(k'_{\text{abs}}+4\pi\right)}{\left(1-\frac{M\pi\left(a'_{\text{abs}}\right)^2}{4\pi}\right)\left(\pi a'_{\text{abs}}k'_{\text{abs}}+16\pi\right)+M\left(a'_{\text{abs}}\right)^2\left(k'_{\text{abs}}+4\pi\right)}, \tag{27}$$

where M is the total number of harvesting units on the surface of the transmitter. Specifically, $k^{\star}_{\text{abs}}$ is substituted instead of k'_{abs} in (23), (24), (25), and (26).

IV. EXPECTED RECEIVED AND HARVESTED SIGNAL MODELS

In this section, we derive mathematical expressions for the dimensionless expected (average) received signal at the receiver, denoted by $N'(t')$, and the dimensionless average harvested signal at the transmitter, denoted by $N'_{\text{Harv}}(t')$, during a dimensionless symbol duration T'_{sym}, assuming that the transmitter releases A molecules with dimensionless rate $\mu'(t')$. In the following, for compactness, we drop the term "dimensionless" when we refer to dimensionless parameters, wherever possible without causing ambiguity.

A. TRANSMITTER RELEASE RATE MODELING

In nature, signaling molecules that are released from biological cells can follow very complex temporal release patterns. For instance, it is shown in [36] that the concentration of neurotransmitters inside the vesicle carrying the neurotransmitters decreases approximately exponentially as a function of time when the vesicle fuses with the pre-synaptic membrane and opens to release the neurotransmitters. However, in this paper, we focus on *linear* release patterns, i.e., we assume that $\mu'(t') = \mu'_0 + q't'$, where μ'_0 is an arbitrary positive constant and q' determines the slope of $\mu'(t')$. The reasons for adopting a linear release pattern are two fold. First, the linear release pattern facilitates the derivation of closed-form expressions for $N'(t')$ and $N'_{\text{Harv}}(t')$. Second, both the complex theoretical models developed so far for the release patterns of natural biological systems [16], [20], [36] and experimentally obtained release patterns [24] can be well approximated by piece-wise linear functions.[7] Thus, we model the release pattern of the considered system as follows

$$\mu'(t') = \begin{cases} \mu'_0 + q't' & \text{if } t'_0 \le t' \le T'_{\text{on}} + t'_0 \\ 0 & \text{if } T'_{\text{on}} + t'_0 \le t' \le T'_{\text{on}} + t'_0 + T'_{\text{off}}. \end{cases} \tag{28}$$

Remark 1: The special case of a *constant* release can be modeled by (28) after setting $q' = 0$.

B. EXPECTED RECEIVED SIGNAL

Now, we focus on the derivation of $N'(t')$ based on $P'_A(t'|r'_0)$. As $P'_A(t'|r'_0)$ is the channel impulse response of the system, $N'(t')$ can be evaluated via the convolution of $P'_A(t'|r'_0)$ and $\mu'(t')$ as follows

$$N'(t') = P'_A(t'|r'_0) * \mu'(t') = \int_{t'_0}^{\infty} P'_A(\tau'|r'_0)\mu'(t'-\tau')\mathrm{d}\tau', \tag{29}$$

where $*$ denotes convolution. In (29), due to the limited duration of function $\mu'(t')$, $N'(t')$ can be split into two parts namely, $N'_{\text{on}}(t')$ and $N'_{\text{off}}(t')$, where $N'_{\text{on}}(t')$ is the solution for $t'_0 \le t' < T'_{\text{on}} + t'_0$, i.e., $N'_{\text{on}}(t') = \int_{t'_0}^{t'} P'_A(\tau'|r'_0)\mu'(t'-\tau')\mathrm{d}\tau'$, whereas $N'_{\text{off}}(t')$ is the solution for $T'_{\text{on}} + t'_0 \le t' \le T'_{\text{on}} + t'_0 + T'_{\text{off}}$, i.e., $N'_{\text{off}}(t') = \int_{t'-T'_{\text{on}}-t'_0}^{t'} P'_A(\tau'|r'_0)\mu'(t'-\tau')\mathrm{d}\tau'$. The solution of (29) for the linear release rate $\mu'(t')$ in (28) and $P'_A(t'|r'_0)$ in (25) is provided in the following theorem.

Theorem 2 (Expected Received Signal): The expected received signal at a passive receiver located at dimensionless distance r'_{rx} from the center of a harvesting transmitter releasing signaling A molecules with the dimensionless release rate $\mu'(t')$, given in (28), where every released molecule may undergo either one of the two reactions introduced in (1) and (2), is given by

$$N'_{\text{on}}(t') = \Psi\big|_{\tau'=t'} - \Psi\big|_{\tau'=t'_0}, \quad t'_0 \le t' < T'_{\text{on}} + t'_0$$
$$N'_{\text{off}}(t') = \Psi\big|_{\tau'=t'} - \Psi\big|_{\tau'=t'-T'_{\text{on}}-t'_0}, \quad T'_{\text{on}} + t'_0 \le t' \le T'_{\text{on}} + t'_0 + T'_{\text{off}} \tag{30}$$

where Ψ is defined as follows

$$\Psi = \Psi_1 - q'\varepsilon'(\Psi_{21} + \Psi_{22}). \tag{31}$$

Here, we define $\varepsilon' = \frac{V_{\text{rx}}}{4\pi(r'_{\text{rx}})}$, and Ψ_1, Ψ_{21}, and Ψ_{22} are given in (32), (33), and (34), shown at the bottom of the next page, respectively.

Proof: The proof is provided in Appendix B. ■

In the following, we analyze some special cases of the expected received signal.

Corollary 1 (Constant Release With Degradation): For this special case Ψ in (31) reduces to $\Psi = \Psi_1$. This result can be easily obtained after setting $q' = 0$ in (31).

Corollary 2 (Constant Release Without Degradation): For constant release of the signaling molecules by the transmitter and no degradation reaction in the channel, Ψ in (31) is obtained as follows

6. We refer the interested reader to [30] for the detailed derivation of the modified reaction rate constant.

7. Theoretical and experimental release patterns potentially can take the followings effects into account: 1) signaling molecule generation (e.g., via chemical reaction networks) at a given location *inside* the transmitter at a certain distance from the surface, 2) transportation of the generated signaling molecules (e.g., via diffusion or molecular motors) to the surface of the transmitter, and 3) mechanisms that control the release of the signaling molecules (e.g., voltage-gated ion channels). To facilitate the analysis of the end-to-end MC system, the resulting highly non-linear release patterns can be approximated by the piece-wise linear release patterns considered in this paper.

$$\Psi = \Psi_1\Big|_{k'_{\rm d}\to 0} = \frac{\varepsilon'\mu'_0}{\alpha'}\Bigg[-\mathrm{erf}\left(\frac{r'_{\rm rx}-1}{\sqrt{4\tau'}}\right) - \exp\big(\alpha'\big(r'_{\rm rx}-1\big) + (\alpha')^2\tau'\big)\mathrm{erfc}\left(\frac{r'_{\rm rx}-1}{\sqrt{4\tau'}} + \alpha'\sqrt{\tau'}\right)\Bigg]. \tag{35}$$

For the special cases considered in Corollaries 1 and 2, $N'(t')$ scales linearly with $\mu'(t')$. Furthermore, Corollary 2 shows that for constant release without degradation the behavior of $N'(t')$ for large times can be approximated with the first term ($\mathrm{erf}(\cdot)$) in the brackets in (35), as the second term approaches zero.

We note that the expression derived for the expected received signal in (30) is complex and may not provide immediate meaningful insights about the interplay of the different system parameters influencing $N'(t')$. However, two main benefits of the expressions in (30)-(34) are as follows;

- The time needed for evaluation of (30)-(34) is less than that needed for a particle-based simulation. For particle-based simulation, the positions of individual signaling molecules and their interactions with other entities in the environment must be tracked over time. This makes particle-based simulations computationally very expensive and also time inefficient. Moreover, for assessing the performance of MC systems, we are typically interested in the evaluation of the corresponding bit/symbol error rates, which requires the transmission of several thousands of symbols. This requirement makes particle-based simulations even more inefficient for evaluation of the symbol/bit error rate of MC systems. On the other hand, the expressions in (30)-(34) can be calculated once, stored offline, and employed for Monte Carlo simulation of symbol/bit error rate.
- $N'(t')$ can be employed for parameter estimation problems in MC systems. In particular, when $N'(t')$ in (30) is

$$\Psi_1 = \varepsilon'\big(\mu'_0 + q't'\big)\Bigg[\frac{-\alpha' e^{-k'_{\rm d}\tau'}}{\big((\alpha')^2 - k'_{\rm d}\big)}\exp\big(\alpha'\big(r'_{\rm rx}-1\big) + (\alpha')^2\tau'\big)\mathrm{erfc}\left(\frac{r'_{\rm rx}-1}{\sqrt{4\tau'}} + \alpha'\sqrt{\tau'}\right) - \frac{e^{-(r'_{\rm rx}-1)\sqrt{k'_{\rm d}}}}{2\big(\alpha' + \sqrt{k'_{\rm d}}\big)}$$
$$\times\ \mathrm{erf}\left(\frac{r'_{\rm rx}-1}{\sqrt{4\tau'}} - \sqrt{k'_{\rm d}\tau'}\right) - \frac{e^{(r'_{\rm rx}-1)\sqrt{k'_{\rm d}}}}{2\big(\alpha' - \sqrt{k'_{\rm d}}\big)}\left(\mathrm{erf}\left(\frac{r'_{\rm rx}-1}{\sqrt{4\tau'}} + \sqrt{k'_{\rm d}\tau'}\right) - 1\right) - \frac{e^{-(r'_{\rm rx}-1)\sqrt{k'_{\rm d}}}}{2\big(\alpha' - \sqrt{k'_{\rm d}}\big)}\Bigg] \tag{32}$$

where $\mathrm{erf}(\cdot)$ is the error function.

$$\Psi_{21} = \frac{-e^{-\sqrt{k'_{\rm d}}(r'_{\rm rx}-1)}}{4k'_{\rm d}\sqrt{k'_{\rm d}}}\Bigg[\Big(\sqrt{k'_{\rm d}}\big(r'_{\rm rx}-1\big)+1\Big)\mathrm{erf}\left(\frac{r'_{\rm rx}-1}{\sqrt{4\tau'}} - \sqrt{k'_{\rm d}\tau'}\right) + \Big(\sqrt{k'_{\rm d}}\big(r'_{\rm rx}-1\big)-1\Big)\Big(e^{2\sqrt{k'_{\rm d}}(r'_{\rm rx}-1)}$$
$$\times\ \mathrm{erf}\left(\frac{r'_{\rm rx}-1}{\sqrt{4\tau'}} + \sqrt{k'_{\rm d}\tau'}\right) - e^{2\sqrt{k'_{\rm d}}(r'_{\rm rx}-1)} + 1\Big)\Bigg] - \frac{1}{\sqrt{\pi}k'_{\rm d}}\sqrt{\tau'}\exp\left(\frac{-\big(r'_{\rm rx}-1\big)^2}{4\tau'} - k'_{\rm d}\tau'\right) \tag{33}$$

$$\Psi_{22} = \Bigg[\frac{\alpha' e^{-\sqrt{k'_{\rm d}}(r'_{\rm rx}-1)}}{2\big(\alpha' + \sqrt{k'_{\rm d}}\big)\sqrt{k'_{\rm d}}}\left(\tau' + \frac{\alpha'}{\big((\alpha')^2 - k'_{\rm d}\big)} + \frac{\Big(2\sqrt{k'_{\rm d}}\big(r'_{\rm rx}-1\big)+1\Big)}{4\sqrt{k'_{\rm d}}}\right) + \frac{\alpha' e^{-\sqrt{k'_{\rm d}}(r'_{\rm rx}-1)}}{8k'_{\rm d}\big(\alpha' - \sqrt{k'_{\rm d}}\big)\sqrt{k'_{\rm d}}}\Bigg]\times\mathrm{erf}\left(\frac{r'_{\rm rx}-1}{\sqrt{4\tau'}} - \sqrt{k'_{\rm d}\tau'}\right)$$
$$+ \Bigg[\frac{\alpha' e^{\sqrt{k'_{\rm d}}(r'_{\rm rx}-1)}\Big(2\sqrt{k'_{\rm d}}\big(r'_{\rm rx}-1\big)-1\Big)}{8k'_{\rm d}\big(\alpha' - \sqrt{k'_{\rm d}}\big)\sqrt{k'_{\rm d}}} - \frac{\alpha' e^{\sqrt{k'_{\rm d}}(r'_{\rm rx}-1)}}{8k'_{\rm d}\big(\alpha' + \sqrt{k'_{\rm d}}\big)\sqrt{k'_{\rm d}}} - \left(\tau' + \frac{\alpha'}{\big((\alpha')^2 - k'_{\rm d}\big)}\right)\left(\frac{\alpha' e^{\sqrt{k'_{\rm d}}(r'_{\rm rx}-1)}}{2\big(\alpha' - \sqrt{k'_{\rm d}}\big)\sqrt{k'_{\rm d}}}\right)\Bigg]$$
$$\times\left(\mathrm{erf}\left(\frac{r'_{\rm rx}-1}{\sqrt{4\tau'}} + \sqrt{k'_{\rm d}\tau'}\right) - 1\right) - \frac{\alpha' e^{-\sqrt{k'_{\rm d}}(r'_{\rm rx}-1)}\tau'}{2\big(\alpha' + \sqrt{k'_{\rm d}}\big)\sqrt{k'_{\rm d}}}\mathrm{erf}\left(\frac{r'_{\rm rx}-1}{\sqrt{4\tau'}} - \sqrt{k'_{\rm d}\tau'}\right) - \frac{e^{\sqrt{k'_{\rm d}}(r'_{\rm rx}-1)}\tau'}{2\big(\alpha' - \sqrt{k'_{\rm d}}\big)\sqrt{k'_{\rm d}}}$$
$$\times\ \mathrm{erfc}\left(\frac{r'_{\rm rx}-1}{\sqrt{4\tau'}} + \sqrt{k'_{\rm d}\tau'}\right) + \frac{\big(\alpha'\big)^2\sqrt{\tau'}}{k'_{\rm d}\sqrt{\pi}\big((\alpha')^2 - k'_{\rm d}\big)}\exp\left(-\frac{\big(r'_{\rm rx}-1\big)^2}{4\tau'} - k'_{\rm d}\tau'\right) - \left(\tau' + \frac{\alpha'}{\big((\alpha')^2 - k'_{\rm d}\big)}\right)\frac{\alpha' e^{-k'_{\rm d}\tau'}}{\big((\alpha')^2 - k'_{\rm d}\big)}$$
$$\times\ \exp\Big(\big(\alpha'\big)^2\tau' + \alpha'\big(r'_{\rm rx}-1\big)\Big)\mathrm{erfc}\left(\frac{r'_{\rm rx}-1}{\sqrt{4\tau'}} + \alpha'\sqrt{\tau'}\right) - \frac{\alpha' e^{-\sqrt{k'_{\rm d}}(r'_{\rm rx}-1)}}{8k'_{\rm d}\big(\alpha' + \sqrt{k'_{\rm d}}\big)\sqrt{k'_{\rm d}}} - \frac{(\alpha')^2 e^{-\sqrt{k'_{\rm d}}(r'_{\rm rx}-1)}}{2\big(\alpha' - \sqrt{k'_{\rm d}}\big)\sqrt{k'_{\rm d}}\big((\alpha')^2 - k'_{\rm d}\big)}$$
$$+ \frac{\alpha' e^{-\sqrt{k'_{\rm d}}(r'_{\rm rx}-1)}\Big(2\sqrt{k'_{\rm d}}\big(r'_{\rm rx}-1\big)-1\Big)}{8k'_{\rm d}\big(\alpha' - \sqrt{k'_{\rm d}}\big)\sqrt{k'_{\rm d}}} \tag{34}$$

converted into its dimensional form, it can be employed for estimation of parameters (individually or jointly) such as the distance between transmitter and receiver, diffusion coefficient of signaling molecules, degradation reaction constant, molecule release rate, etc. We refer the interested reader to [37] for parameter estimation techniques in MC systems.

C. EXPECTED HARVESTED SIGNAL

In this section, we calculate $N'_{\text{Harv}}(t')$ based on the *harvested impulse response* $P'^{\text{Harv}}_A(t'|r'_0)$ in (26). Similar to the evaluation of $N'(t')$, $N'_{\text{Harv}}(t')$ is obtained by convolving $\mu'(t')$ and $P'^{\text{Harv}}_A(t'|r'_0)$, i.e.,

$$\begin{aligned} N'_{\text{Harv}}(t') &= P'^{\text{Harv}}_A(t'|r'_0) * \mu'(t') \\ &= \int_{t'_0}^{\infty} P'^{\text{Harv}}_A(\tau'|r'_0)\mu'(t'-\tau')\mathrm{d}\tau'. \end{aligned} \tag{36}$$

Here, we split $N'_{\text{Harv}}(t')$ into two parts, i.e., $N'_{\text{Harv, on}}(t')$ and $N'_{\text{Harv, off}}(t')$. In particular, $N'_{\text{Harv, on}}(t')$ and $N'_{\text{Harv, off}}(t')$ are the solutions of the convolution in (36) for dimensionless times $t'_0 \le t' \le T'_{\text{on}} + t'_0$ and $T'_{\text{on}} + t'_0 \le t' \le T'_{\text{on}} + t'_0 + T'_{\text{off}}$, respectively. The solution of (36) for the linear release rate $\mu'(t')$ given in (28) and $P'^{\text{Harv}}_A(t'|r'_0)$ in (26) is provided in the following theorem.

Theorem 3 (Expected Harvested Signal): The expected harvested signal at a molecule harvesting transmitter releasing signaling A molecules with the dimensionless release rate $\mu'(t')$, given in (28), where every released molecule may undergo either one of the two reactions introduced in (1) and (2), is given as follows

$$\begin{aligned} N'_{\text{Harv,on}}(t') &= \Xi\big|_{\tau'=t'} - \Xi\big|_{\tau'=t'_0}, \quad t'_0 \le t' \le T'_{\text{on}} + t'_0 \\ N'_{\text{Harv,off}}(t') &= \Xi\big|_{\tau'=t'} - \Xi\big|_{\tau'=t'-T'_{\text{on}}-t'_0}, \\ &\quad T'_{\text{on}} + t'_0 \le t' \le T'_{\text{on}} + t'_0 + T'_{\text{off}} \end{aligned} \tag{37}$$

where Ξ is defined as

$$\Xi = \Xi_1 - q'\Xi_2. \tag{38}$$

Here, Ξ_1 and Ξ_2 are defined in (39) and (40), shown at the bottom of the page, respectively.

Proof: The proof is provided in Appendix C. ■

We note that based on the definition of $P'^{\text{Harv}}_A(\tau'|r'_0)$ provided in (12), i.e., $P'^{\text{Harv}}_A(\tau'|r'_0)$ being the probability of harvesting a given A molecule *until* time t', $N'_{\text{Harv}}(t')$ represents the *accumulated* number of harvested molecules. As a consequence, given $N'_{\text{Harv}}(t')$, we can calculate the total number of harvested A molecules during small observation window $\Delta t'$ as follows

$$\tilde{N}'_{\text{Harv}}(t') = \frac{N'_{\text{Harv}}(t'+\Delta t') - N'_{\text{Harv}}(t')}{\Delta t'}. \tag{41}$$

In the following, we refer to $\tilde{N}'_{\text{Harv}}(t')$ as the average molecule harvesting rate.

In the following, we analyze some special cases of the expected harvested signal.

Corollary 3 (Constant Release With Degradation): For this special case, Ξ in (38) reduces to $\Xi = \Xi_1$. This result can be easily obtained by setting $q' = 0$ in (38).

Corollary 4 (Constant Release Without Degradation): For the constant release of signaling molecules by the transmitter and no degradation reaction in the channel, Ξ in (38) can be obtained as follows

$$\begin{aligned} \Xi = \frac{k'_{\text{abs}}\mu'_0}{4\pi}\Bigg[\frac{-1}{(\alpha')^3}\Big(&\exp\Big((\alpha')^2\tau'\Big) \\ &\times \operatorname{erfc}\left(\alpha'\sqrt{\tau'}\right) + \frac{2\alpha'\tau'}{\sqrt{\pi}}\Big) + \frac{\tau'}{\alpha'}\Bigg]. \end{aligned} \tag{42}$$

Proof: Eq. (42) is obtained by evaluating Ξ_1 in the limit of $k'_{\text{d}} \to 0$. ■

$$\begin{aligned} \Xi_1 = \frac{k'_{\text{abs}}\left(\mu'_0 + q't'\right)}{4\pi}\Bigg[&\frac{-\alpha'}{\left((\alpha')^2 - k'_{\text{d}}\right)^2}\left(\exp\Big((\alpha')^2\tau' - k'_{\text{d}}\tau'\Big)\operatorname{erfc}\left(\alpha'\sqrt{\tau}\right) + \frac{\alpha'}{\sqrt{k'_{\text{d}}}}\operatorname{erf}\left(\sqrt{k'_{\text{d}}\tau'}\right)\right) + \frac{\sqrt{k'_{\text{d}}}}{(\alpha')^2 - k'_{\text{d}}} \\ &\times \left(\frac{\operatorname{erf}\left(\sqrt{k'_{\text{d}}\tau'}\right)}{2k'_{\text{d}}} - \frac{\sqrt{\tau'}\exp\left(-k'_{\text{d}}\tau'\right)}{\sqrt{\pi k'_{\text{d}}}} + \tau'\operatorname{erfc}\left(\sqrt{k'_{\text{d}}\tau'}\right)\right) + \frac{\tau'}{\alpha' + k'_{\text{d}}}\Bigg] \end{aligned} \tag{39}$$

$$\begin{aligned} \Xi_2 = \frac{k'_{\text{abs}}}{4\pi}\Bigg[&\frac{-\alpha'}{\left((\alpha')^2 - k'_{\text{d}}\right)^3}\Bigg\{\frac{-1}{\sqrt{\pi}\left(k'_{\text{d}}\tau'\right)^{3/2}}\Bigg[\alpha'(\tau')^{3/2}\Big((\alpha')^2 - k'_{\text{d}}\Big)\left(e^{-k'_{\text{d}}\tau'}\sqrt{k'_{\text{d}}\tau'} - \frac{\sqrt{\pi}}{2}\left(\operatorname{erf}\left(\sqrt{k'_{\text{d}}\tau'}\right) - 1\right)\right)\Bigg] \\ &+ \exp\Big(\Big((\alpha')^2 - k'_{\text{d}}\Big)\tau'\Big)\operatorname{erfc}\left(\alpha'\sqrt{\tau'}\right)\Big((\alpha')^2\tau' - k'_{\text{d}}\tau' - 1\Big) - \frac{\alpha'}{\sqrt{k'_{\text{d}}}}\operatorname{erf}\left(\sqrt{k'_{\text{d}}\tau'}\right)\Bigg\} + \frac{\sqrt{k'_{\text{d}}}}{8\Big((\alpha')^2 - k'_{\text{d}}\Big)} \\ &\times \left\{\frac{3}{\left(k'_{\text{d}}\right)^2} \times \operatorname{erf}\left(\sqrt{k'_{\text{d}}\tau'}\right) - \frac{2\sqrt{\tau'}}{\sqrt{\pi}\left(k'_{\text{d}}\right)^{3/2}}e^{-k'_{\text{d}}\tau'}\left(2k'_{\text{d}}\tau' + 3\right) + 4(\tau')^2\operatorname{erfc}\left(\sqrt{k'_{\text{d}}\tau'}\right)\right\} + \frac{(\tau')^2}{2(\alpha' + \sqrt{k'_{\text{d}}})}\Bigg] \end{aligned} \tag{40}$$

Corollary 5 (Linear Release Without Degradation): For the linear release of signaling molecules by the transmitter and no degradation reaction in the channel, Ξ is given by (38), where Ξ_1 is reduced to (42) and Ξ_2 is given by

$$\Xi_2 = \frac{-k'_{\rm abs}}{4\pi\alpha'}\left[\frac{1}{(\alpha')^4}\exp\Big((\alpha')^2\tau'\Big)\text{erfc}\left(\alpha'\sqrt{\tau'}\right)\right.$$
$$\left.\times\left((\alpha')^2\tau'-1\right)+\frac{2\sqrt{\tau'}\Big((\alpha')^2\tau'-3\Big)}{3\sqrt{\pi}(\alpha')^3}-\frac{(\tau')^2}{2}\right]. \tag{43}$$

Proof: Eq. (43) is obtained by evaluating Ξ_2 in the limit of $k'_{\rm d}\to 0$. ■

We can observe from Corollaries 3, 4, and 5 that for all these special cases, $N'_{\rm Harv}(t')$ scales linearly with $\mu'(t')$. Also, for the case of constant release with $k'_{\rm d}=0$, for large τ', Ξ in (42) scales linearly with τ', while Ξ_2 in (43) scales with $(\tau')^2$.

The expression obtained for the expected harvested signal in (37), similar to (30), is very involved and may not provide meaningful insight at first. However, two main benefits of the closed-form expressions in (37)-(40) are as follows.

- The time needed for evaluation of the expressions in (37)-(40) is less than that needed for corresponding particle-based simulations. As explained before, the expected harvest signal can be computed once, stored offline, and employed for Monte Carlo simulations.
- When the expressions in (37)-(40) are converted to their dimensional form, they can be employed for parameter estimation at the transmitter. Generally, parameter estimation and CSI acquisition at the *transmitter* has not been studied for MC systems so far, due to the simplistic adopted transmitter models. However, the transmitter model developed in this work, enables channel parameter estimation and CSI acquisition at the *transmitter*. In conventional communication systems, the CSI acquisition is performed at the receiver and provided to the transmitter via a feedback channel. However, in MC systems, due to the slow motion of signaling molecules, relying on a feedback channel may not be a feasible solution for obtaining CSI at the transmitter. For instance, when the parameters of the channel, such as the viscosity, temperature, and distance between transmitter and receiver change over time, the CSI acquired at the receiver may become outdated by the time it is received at the transmitter via a feedback channel. Thus, having transmitter models that are capable of CSI acquisition and/or estimating the parameters of the channel at the transmitter itself are of particular importance for MC system design. The transmitter models developed in this work constitute a crucial first step towards the realization of this objective.

V. SIMULATION RESULTS

In this section, we present simulation and analytical results for evaluation of the accuracy of the derived closed-form expressions for the expected received and harvested signals, respectively. The particle-based simulations are performed based on the algorithm introduced in [30, Sec. V].

TABLE 1. Simulation parameters.

Parameter	Value	Parameter	Value
$a_{\rm tx}$	$0.25\,\mu$m	$a'_{\rm abs}$	0.0558
$a_{\rm rx}$	$0.25\,\mu$m	D_A	$1\times10^{-8}\,\frac{\rm m^2}{\rm s}$ ms
M	4000	$U_{\max}$	4000

For our simulations, we adopted the parameters in Table 1. In addition, we further assume that for a given $\mu(t)$, every release unit releases A molecules with a rate of $\mu(t)/U_{\max}$. This assumption makes the results provided in this section independent of $U_{\max}$ as far as $\mu(t)$ is concerned. Finally, the symbol duration $T'_{\rm sym}$ is chosen equal to the entire simulation time. The only parameters that are varied are $k'_{\rm d}$, $k'_{\rm abs}$, $\mu'(t)$, and $T'_{\rm on}$. The simulation results are averaged over 10^4 independent realizations and a simulation step size of 5×10^{-9}s was chosen. Before discussing the provided results in detail, we note that all analytical results shown in Figs. 3-8 are in excellent agreement with the corresponding simulation results.[8] In the following, the simulation results for the expected received signal and the expected harvested signal are provided in Sections V-A and V-B, respectively.

A. EXPECTED RECEIVED SIGNAL

In this subsection, we assess the accuracy of the analytical expression derived for the received signal $N'(t')$ and provide insight regarding some design aspects of synthetic MC systems.

In Fig. 3, $N'(t')$ is plotted as a function of dimensionless time t' for the system parameters in Table 1 and the constant release scenario, i.e., $q'=0$, with $\mu_0=2\times10^9\ \frac{\rm molecule}{\rm s}$ ($\mu'_0=3150.05$).

In Fig. 3a, the impact of the harvesting reaction rate on the received signal is shown. It is assumed that the transmitter releases molecules during the entire symbol duration, i.e., $T'_{\rm on}=T'_{\rm sym}$, $k'_{\rm abs}=\{0,2,4,8\}$, and $k'_{\rm d}=0$. As can be seen, for all values of $k'_{\rm abs}$, $N'(t')$ is an increasing function of t' during $T'_{\rm sym}$. This is because, unlike for an impulsive release, here signaling molecules are continuously released by the transmitter. Furthermore, as can be observed, for larger values of $k'_{\rm abs}$, the magnitude of the received signal decreases, as for larger $k'_{\rm abs}$, more molecules are harvested by the transmitter and, consequently, fewer molecules arrive at the receiver.

8. We note that the simulation parameters are chosen to minimize the computational time required for stochastic simulation of the diffusion process and the chemical reactions. However, based on the dimensionless analysis provided in Section III-C, the simulation results can be easily scaled to reflect practical values for the simulation parameters. For instance, adopting the diffusion coefficient of neurotransmitter particles reported in [23] ($D_{\rm NT}=3.3\times10^{-10}\,\frac{\rm m^2}{\rm s}$), the dimensionless time t' axis for all simulation results in this section is scaled by a factor of 3.3×10^{-2}.

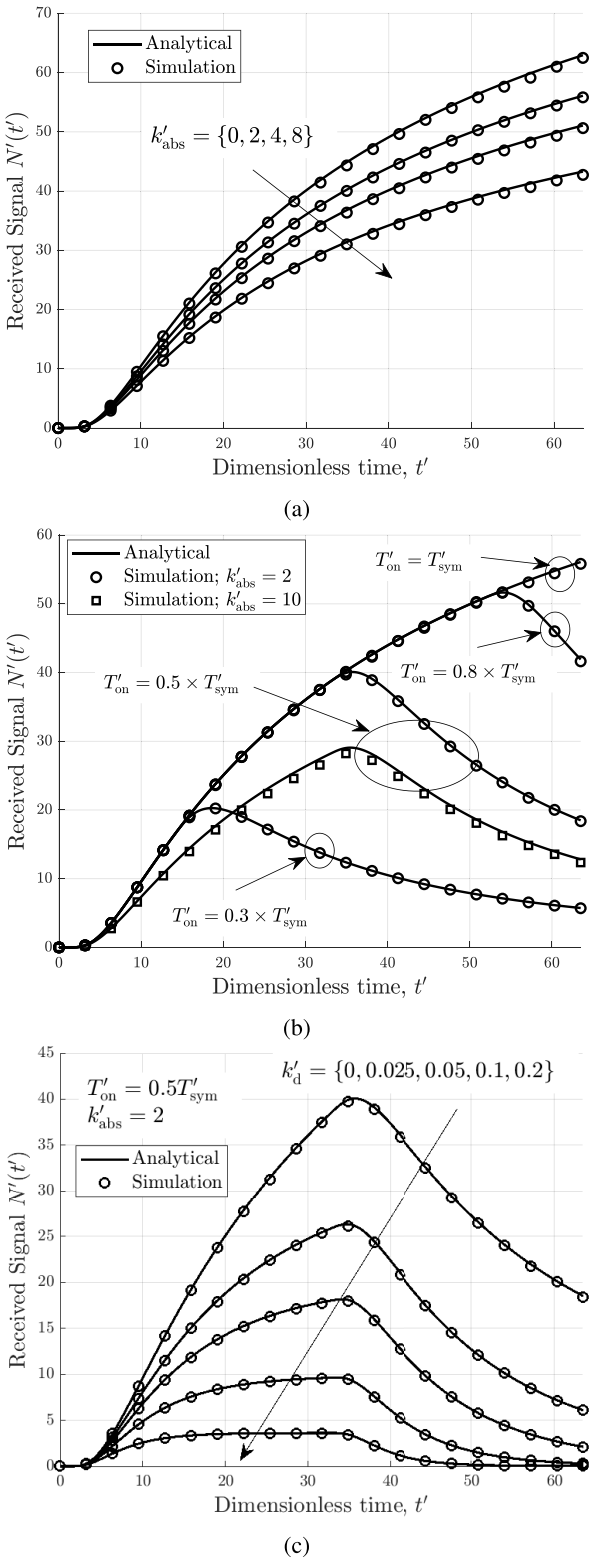

FIGURE 3. $N'(t')$ as a function of t'; impact of (a) k'_{abs}, (b) T'_{on}, and (c) k'_d.

Fig. 3b shows the impact of the duration of the molecule release, T'_{on}, on the received signal. For Fig. 3b, it is assumed that $k'_{abs} = \{2, 10\}$, $k'_d = 0$, and the release duration is chosen as $T'_{on} = \{1, 0.8, 0.5, 0.3\} \times T'_{sym}$. As can be seen in Fig. 3b, for all cases, $N'(t')$ first increases for $t' \leq T'_{on}$ and then decreases for $t' > T'_{on}$. Moreover, for smaller T'_{on}, both the maximum number of observed molecules and the time instant when the maximum occurs decreases. Also, when $T'_{on} = 0.5 \times T'_{sym}$, we can observe that by increasing k'_{abs} from 2 to 10, the magnitude of the received signal is decreased in both time intervals, i.e., $t' \leq T'_{on}$ and $t' \geq T'_{on}$.

Fig. 3c studies the impact of degradation reaction rate k'_d on the received signal. Here, we adopt $k'_{abs} = 2$ and $T'_{on} = 0.5T'_{sym}$, and $k'_d = \{0, 0.025, 0.05, 0.1, 0.2\}$ is varied. As can be observed in Fig. 3c, in case of degradation, i.e., $k'_d > 0$, the magnitude of the received signal is smaller during the entire range of times considered compared to the case where $k'_d = 0$. This reduction in the magnitude of the received signal is larger for larger values of k'_d. This is expected since for larger $k'_d > 0$, the probability of degradation in the channel is larger and, as a result, fewer molecules arrive at the receiver. Furthermore, an interesting observation can be made in Fig. 3c. In particular, as k'_d increases, the received signal during T'_{on} becomes flatter. This is due to the fact that for sufficiently large k'_d, the degradation process in the channel and the production process at the transmitter compensate each other.

Some important takeaways from the results provided in Fig. 3 are as follows. First, comparing MH and none-molecule harvesting (N-MH) transmitters, both types of transmitters can control the received signal level at the receiver by adjusting the release duration T'_{on}. However, MH transmitters can also control $N'(t')$ via k'_{abs}. Second, MH transmitters can be effectively employed to improve the communication link reliability by reducing inter-symbol-interference (ISI). In particular, ISI is reduced as the tail of expected received signal is decreased for larger k'_{abs}, see, e.g., Fig. 3b. This leads to less overlap between two consecutive received signals and reduces ISI.

In Fig. 4, $N'(t')$ is depicted as a function of t' for the system parameters in Table 1 and a linearly *increasing* release rate $\mu'(t')$, i.e., $q' > 0$, with $\mu_0 = 2 \times 10^9$ $\frac{\text{molecule}}{\text{s}}$, which corresponds to dimensionless $\mu'_0 = 3150.05$.

In Fig. 4a, the impact of the variation of the release rate $N'(t')$ is studied. We adopted system parameters $T'_{on} = T'_{sym}$, $k'_{abs} = 2$, $k'_d = 0$, and $q = \{0, 1, 2, 3, 4\} \times 10^5$ $\frac{\text{molecule}}{\text{s}^2}$ ($q' = \{0, 1, 2, 3, 4\} \times 49.6141$). Fig. 4a shows that when $q > 0$, $N'(t')$ increases faster with t' compared to the case with $q = 0$. This result is expected since for $q > 0$, more signaling molecules are released by the transmitter over time, and eventually more molecules arrive at the receiver. Furthermore, for a given t', the gap between $N'(t')$ when $q = 0$ and $N'(t')$ when $q > 0$ is larger for larger values of q.

In Fig. 4b, the impact of k'_d on $N'(t')$ is investigated. Here, it is assumed that $T'_{on} = 0.5T'_{sym}$, $k'_{abs} = 2$, and two sets of system parameters are considered. For Set 1, $k'_d = 0.025$ is fixed and $q = \{1, 2, 3, 4\}$ is varied, while for Set 2, $q = 1 \times 10^5$ is kept constant and $k'_d = \{0.05, 0.1, 0.2\}$ is varied.

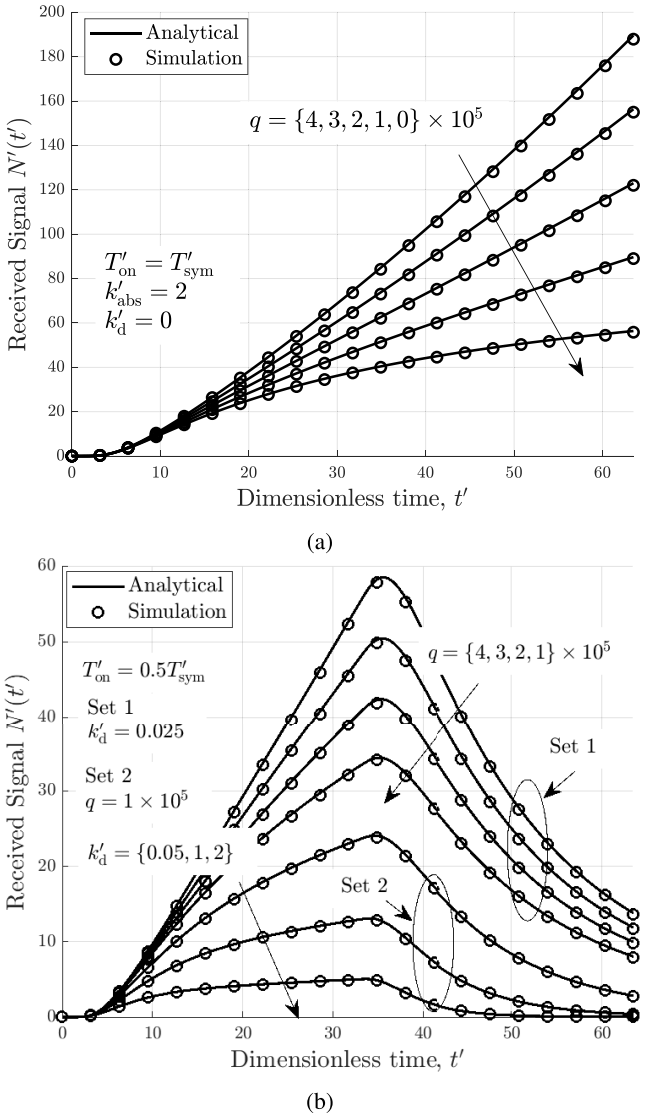

FIGURE 4. $N'(t')$ as a function of t' for linearly increasing release rates $\mu'(t')$.

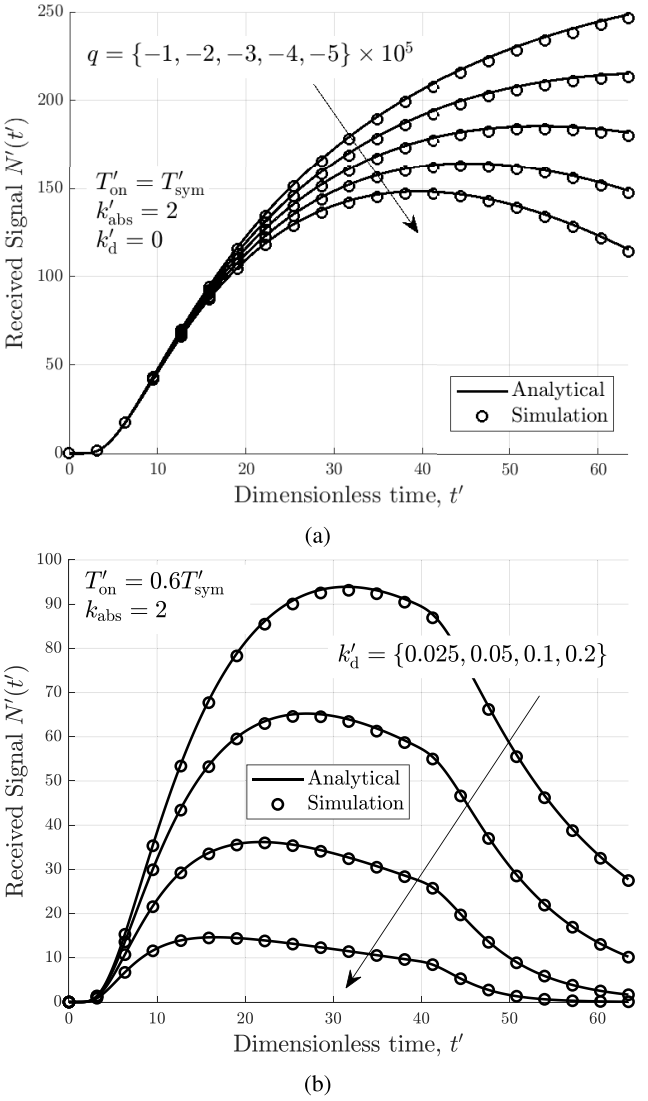

FIGURE 5. $N'(t')$ as a function of t' for linearly decreasing release rate $\mu'(t')$.

First, it can be observed that for all considered cases, i.e., Set 1 and Set 2, $N'(t')$ increases at first and then decreases since $T'_{on} = 0.5T'_{sym}$ is chosen. Second, for Set 1, we can see that by reducing q, $N'(t')$ decreases for the entire range of times considered. Similarly, for Set 2, $N'(t')$ decreases as k'_d increases, since for larger k'_d more signaling molecules are degraded in the channel.

In Fig. 5, $N'(t')$ is depicted as a function of t' for linearly *decreasing* release rate $\mu'(t')$, i.e., $q' < 0$, with $\mu_0 = 10 \times 10^9 \ \frac{\text{molecule}}{\text{s}}$, which corresponds to dimensionless $\mu'_0 = 15750.25$.

In Fig. 5a, the impact of release rate variations on $N'(t')$ is studied for $q < 0$. Specifically, it is assumed that $T'_{on} = T'_{sym}$, $k'_{abs} = 2$, $k'_d = 0$, and $q = \{-1, -2, -3, -4, -5\} \times 10^5 \ \frac{\text{molecule}}{\text{s}^2}$ ($q' = \{-1, -2, -3, -4, -5\} \times 49.6141$). Fig. 5a shows that for all considered cases, $N'(t')$ first increases over time, since it takes some time for the first released molecules to arrive at the receiver. However, eventually $N'(t')$ starts to decrease as fewer molecules are released later in time. Furthermore, the reduction of $N'(t')$ is larger for smaller values of $q < 0$, see, e.g., the curve for $q = -5 \times 10^5$. This is due to the fact that $\mu'(t')$ decreases faster for smaller values of $q < 0$.

In Fig. 5b, the impact of k'_d on $N'(t')$ is studied. Here, we adopt $T'_{on} = 0.6T'_{sym}$, $k'_{abs} = 2$, $q = -5 \times 10^5 \ \frac{\text{molecule}}{\text{s}^2}$ ($q' = -5 \times 49.6141$), and $k'_d = \{0.025, 0.05, 0.1, 0.2\}$. The overall impact of the degradation reaction rate is similar to the cases studied in Figs. 3c, 4b, i.e., degradation reduces $N'(t')$, $0 \leq t' \leq T'_{sym}$, and flattens $N'(t')$, $0 \leq t' < T'_{on}$. However, an interesting observation can be made regarding the interplay between k'_d and $\mu'(t')$ by comparing the results in Figs. 3c, 4b, and 5b. In particular, when $q' = 0$, μ'_0 and k'_d have an opposite impact and compensate each other. This leads to a flat $N'(t')$ curve with *constant* slope, in the interval $0 \leq t' < T'_{on}$, see, e.g., Fig. 3c for $k'_d = 0.2$. When

$q' > 0$, Fig. 4b shows that the production process, $\mu'(t')$, dominates the impact of the degradation process. This leads to a linearly increasing $N'(t')$ curve with a *positive* slope, in the interval $0 \leq t' < T'_{\text{on}}$, see, e.g., Fig. 4b for $k'_{\text{d}} = 0.2$. On the other hand, when $q' < 0$, as in Fig. 5b, the degradation process is dominant over the production process, and leads to a linearly decreasing $N'(t')$ curve with *negative* slope, in the interval $0 \leq t' < T'_{\text{on}}$, see, e.g., Fig. 5b for $k'_{\text{d}} = 0.2$.

Now, we provide some insights for MC design problems based on the results provided in Figs. 4 and 5. In particular, the transmitter model developed in this paper can be exploited for effective system design to compensate the effect of degradation in the channel. For instance, when k'_{d} is changing over time, our developed transmitter model may be employed to adjust the release pattern $\mu'(t')$ over time to maintain a certain magnitude of the received signal at the receiver. Moreover, novel algorithms can be developed to estimate the slope of $N'(t')$ during $0 \leq t' < T'_{\text{on}}$ as a means to obtain information regarding $\mu'(t')$ at the receiver.

B. EXPECTED HARVESTED SIGNAL

In this subsection, we assess the accuracy of the analytical expressions derived for the average harvested signal, $N'_{\text{Harv}}(t')$, and provide some insight for synthetic MC design problems.

In Fig. 6, the impact of different system parameters on the harvested signal, $N'_{\text{Harv}}(t')$, is studied for a constant release rate. Here, the same set of system parameters as for Fig. 3 is assumed.

In Fig. 6a, the impact of the absorption (or harvesting) rate, k'_{abs}, on $N'_{\text{Harv}}(t')$ is investigated. As expected, when $k'_{\text{abs}} = 0$, no signaling molecules are harvested by the transmitter. On the other hand, when $k'_{\text{abs}} > 0$, the probability of harvesting A molecules increases. This probability is larger for larger values of k'_{abs}, which leads to the harvesting of more A molecules. Furthermore, we observe that $N'_{\text{Harv}}(t')$ increases over time due to the cumulative nature of $N'_{\text{Harv}}(t')$. The impact of k'_{d} is illustrated for two choices of $k'_{\text{abs}} = \{2, 4\}$. In particular, the number of harvested A molecules decreases for larger k'_{d}. This is because for larger k'_{d}, the likelihood that a released A molecule degrades between the time of release and the time of harvesting increases.

In Fig. 6b, the impact of the release duration T'_{on} on $N'_{\text{Harv}}(t')$ is shown. It can be observed that for all considered cases, i.e., $T'_{\text{on}} = \{1, 0.8, 0.5, 0.2\} \times T'_{\text{sym}}$, $N'_{\text{Harv}}(t')$ first increases for $0 \leq t' \leq T'_{\text{on}}$, as A molecules constantly enter the channel, and later saturates to a constant value for $t' > T'_{\text{on}}$, as no new A molecule are released by the transmitter and the previously released A molecules that have not been captured yet have diffused away from the transmitter.

The effectiveness of recycling signaling molecules for future transmissions is evident from the results presented in Fig. 6a and Fig. 6b. In particular, in Fig. 6b, for the case $T'_{\text{on}} = 0.5T'_{\text{sym}}$, by the end of the symbol duration (T'_{sym}), the MH transmitter has approximately harvested $N'_{\text{Harv}}(t') = 1.0689 \times 10^4$ signaling molecules. Given that

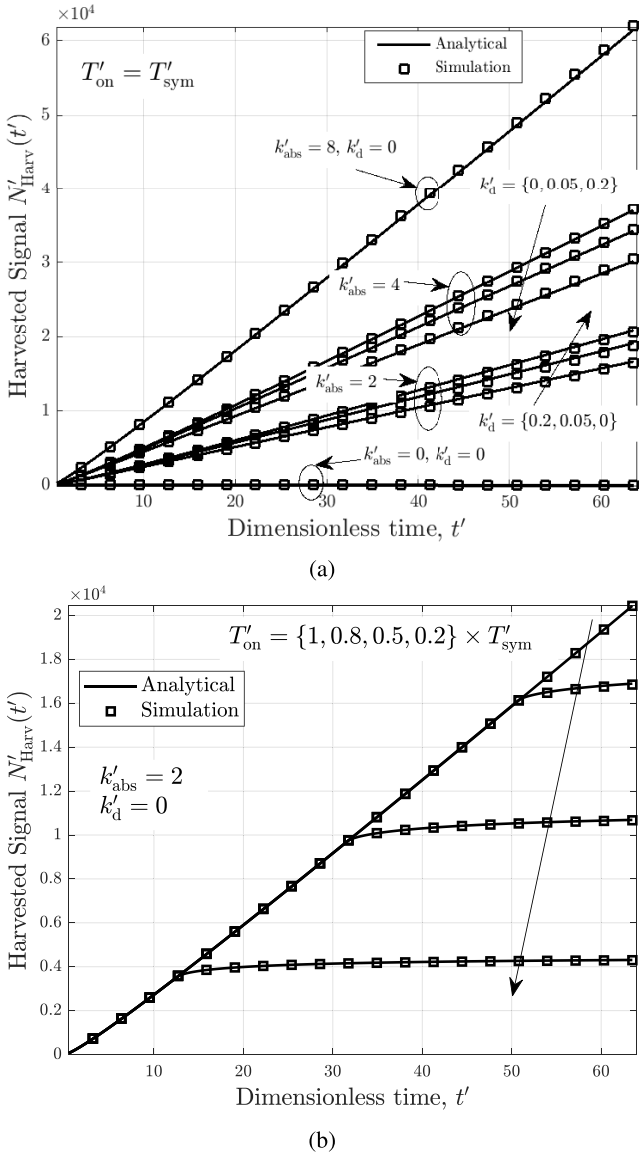

FIGURE 6. $N'_{\text{Harv}}(t')$ as a function of t' for a constant release rate.

for this case $\mu'_0 = 3150.05$ and $q' = 0$, the total number of released molecules during T'_{on} is equal to 1.0001×10^5. This shows that, in every symbol duration, the MH transmitter can recycle $\frac{1.0689 \times 10^4}{1.0001 \times 10^5} = 0.1068$ (10.68%) of the released molecules for future transmissions. The recycling capability can be improved by increasing k'_{abs}. As another example, in Fig. 6a, for the case $T'_{\text{on}} = T'_{\text{sym}}$, $k'_{\text{abs}} = 8$, the MH transmitter harvests approximately $N'_{\text{Harv}}(t') = 6.1460 \times 10^4$ signaling molecules. Given that $\mu'_0 = 3150.05$ and $q' = 0$, the total number of released molecules during $T'_{\text{on}} = T'_{\text{sym}}$ is equal to 2.0003×10^5. Thus, in this case, the MH transmitter can recycle approximately 30.72% of the molecules released in every symbol duration.

In Fig. 7, the impact of different system parameters on the signal harvesting rate, $\tilde{N}'_{\text{Harv}}(t')$, is investigated for linearly *increasing* and *decreasing* release rates, respectively.

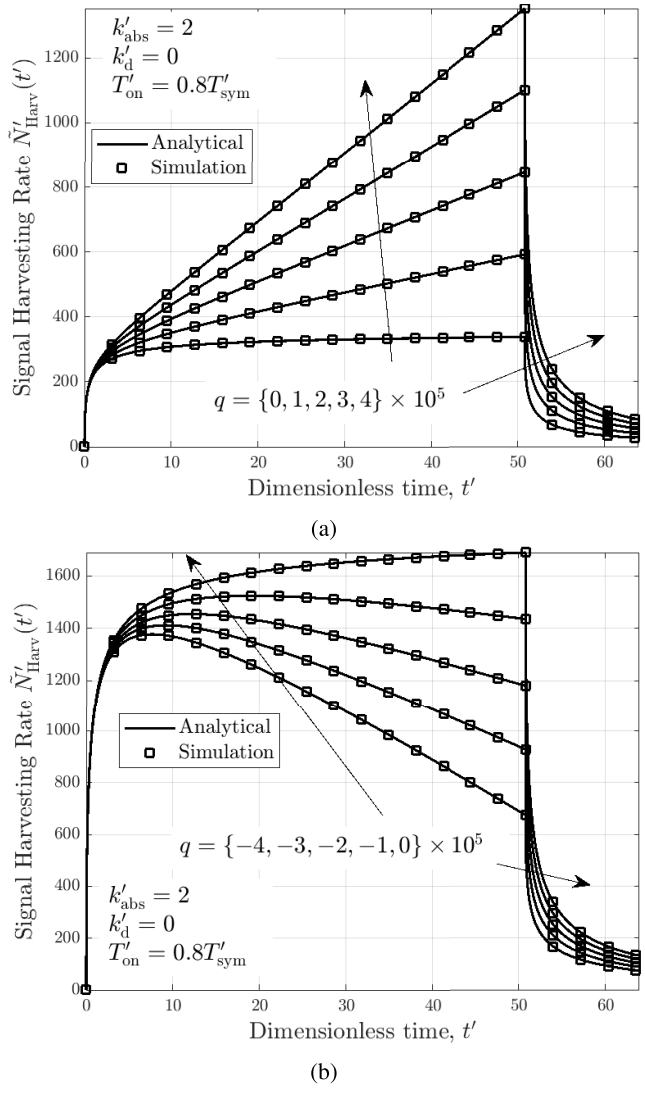

FIGURE 7. $\tilde{N}'_{Harv}(t')$ as a function of t' for linearly increasing or decreasing release rates $\mu'(t')$, respectively.

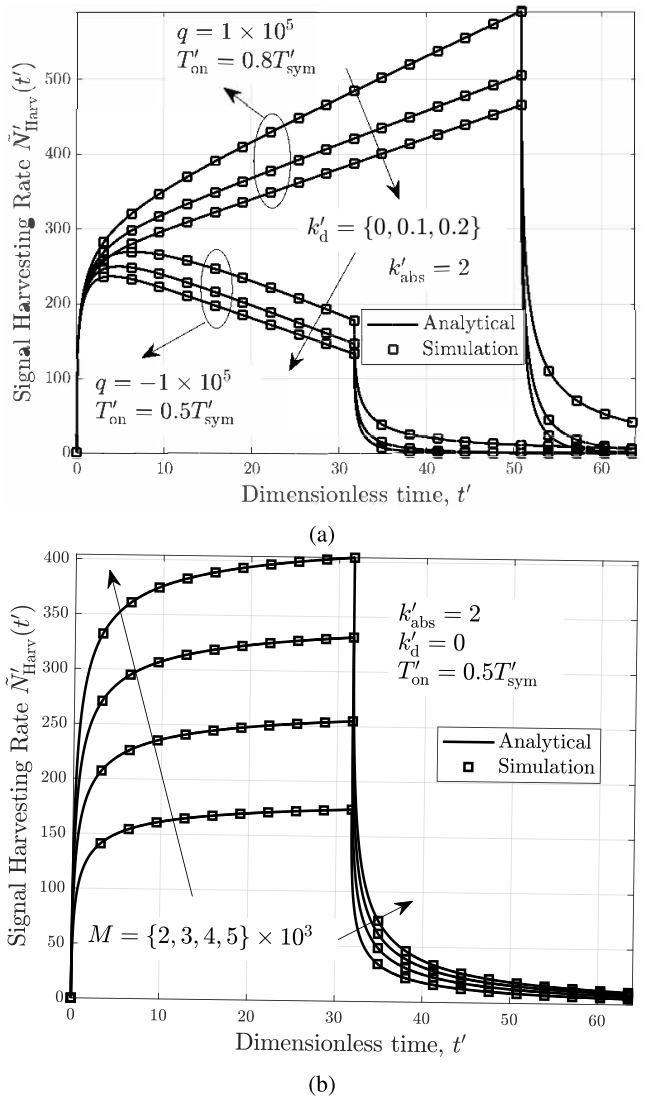

FIGURE 8. $\tilde{N}'_{Harv}(t')$ as a function of t'; impact of k'_d (a) and M (b).

In Fig. 7a, $\tilde{N}'_{Harv}(t')$ is plotted versus t' for the same system parameters as in Fig. 4a, except that T'_{on} is changed to $T'_{on} = 0.8T'_{sym}$. First, when comparing the results of Fig. 7a ($\tilde{N}'_{Harv}(t')$) and Fig. 4a ($N'(t')$), we can observe that the increase of $\tilde{N}'_{Harv}(t')$ immediately after the start of the release of the A molecules is much faster than the increase of $N'(t')$. This is due to the fact that particles released at the transmitter have to diffuse for a longer time to reach the vicinity of the receiver to be observed, while they can potentially be harvested immediately after their release by the transmitter. Second, Fig. 7a shows that for $0 \leq t' \leq T'_{on}$ and when $q = 0$, $\tilde{N}'_{Harv}(t')$ eventually saturates to a constant value. This implies that when the transmitter releases signaling molecules constantly, after an initial transition period, *on average* a constant number of A molecules are harvested. Third, for the case where $q > 0$ and $0 \leq t' \leq T'_{on}$, $\tilde{N}'_{Harv}(t')$ increases over time as $\mu'(t')$ increases. For a given time t', the increase is larger when q is larger. Fourth, it can be observed that for $t' > T'_{on}$, when the transmitter stops releasing new molecules into the channel, the rate at which molecules are harvested decreases sharply.

In Fig. 7b, $\tilde{N}'_{Harv}(t')$ is plotted versus t' for the same system parameters as in Fig. 5a except that T'_{on} is changed to $T'_{on} = 0.8T'_{sym}$. Similar to the curves in Fig. 7a, during $0 \leq t' \leq T'_{on}$, $\tilde{N}'_{Harv}(t')$ increases quickly at first. However, due to the reduction in $\mu'(t')$, $\tilde{N}'_{Harv}(t')$ decreases eventually. The rate of the decrease is faster for smaller values of q, see, e.g., results for $q = -4 \times 10^5$. Furthermore, for $t' > T'_{on}$, $\tilde{N}'_{Harv}(t')$ decreases rapidly.

In Fig. 8a, the impact of k'_d on $\tilde{N}'_{Harv}(t')$ is investigated for two sets of system parameters. For the first set, it is assumed that $q = 1 \times 10^5$ and $T'_{on} = 0.8T'_{sym}$. For the second set, $q = -1 \times 10^5$ and $T'_{on} = 0.5T'_{sym}$ are adopted. For both sets, $k'_{abs} = 2$ and k'_d is changed, i.e., $k'_d = \{0, 0.1, 0.2\}$. As

expected, for both considered parameter sets, $k'_{\rm d} > 0$ leads to a reduction of the harvesting rate of the A molecules. Furthermore, this reduction increases for larger values of $k'_{\rm d}$. Moreover, the above observations are valid during the times when the transmitter releases A molecules and when it is silent.

In Fig. 8b, the impact of the number of harvesting units, M, on $\bar{N}'_{\rm Harv}(t')$ is studied. Here, we assume that $k'_{\rm abs} = 2$, $k'_{\rm d} = 0$, $T'_{\rm on} = 0.5T'_{\rm sym}$, and only $M = \{2, 3, 4, 5\} \times 10^3$ is varied. Fig. 8b clearly shows that by increasing M the average number of harvested A molecules increases. This is due to the fact that by increasing M, the effective area for harvesting signaling molecules on the surface of the transmitter is increased, which, in turn, increases the overall probability of harvesting a given released A molecule.

The results provided in Figs. 6, 7, and 8 reveal one important feature of MH transmitters compared with N-MH transmitters. In particular, MH transmitters can be used to acquire knowledge about the channel (also referred to as channel state information) based on the harvested signal. For instance, based on the developed analytical expressions, novel algorithms for estimation of $k'_{\rm d}$ based on $N'_{\rm Harv}(t')$ at the transmitter can be developed. As can be seen from Fig. 6a, different values of $k'_{\rm d}$ affect the slope of $N'_{\rm Harv}(t')$. Thus, estimating the slope of $N'_{\rm Harv}(t')$ in a certain range allows the transmitter to acquire information regarding the value of $k'_{\rm d}$ in the channel, and then, to adjust the release rate $\mu'(t')$ accordingly. When mathematical expression for the average harvested signal is converted to its dimensional form, potentially, $N'_{\rm Harv}(t')$ can be employed for estimation of other channel parameters such as the diffusion coefficient of the signaling molecules, which also reflects variations in the temperature and/or viscosity of the channel.

VI. CONCLUSION AND FUTURE DIRECTIONS

In this paper, we introduced novel mathematical models for MC transmitters with molecule harvesting capability. In particular, motivated by the existing molecule harvesting mechanisms in nature, we considered a transmitter whose surface is equipped with molecule harvesting units capable of capturing signaling molecules after their release on the surface of the transmitter. Furthermore, we derived closed-form expressions for the average observed signal at the receiver and the average harvested signal at the transmitter assuming a linear release pattern for the signaling molecules. The accuracy of the developed mathematical expressions was confirmed by particle based simulation. Our simulation and analytical results show the intricate interplay of the different parameters on the expected received and harvested signals. For instance, the results revealed the interplay between degradation and production processes, where for linearly increasing (decreasing) release rates, the production (degradation) process dominates the degradation (production) process and leads to a linearly increasing (decreasing) harvested signal rate during the window that transmitter absorbs signaling molecules. Moreover, the results showed that the magnitude of the degradation reaction constant influences the slope of the harvested received signal. This characteristic of the harvested received signal can be exploited for the design of more advance MC transmitters that are cable of probing the environment and adapting their molecule release pattern to the channel conditions.

The development of transmitter architectures that exploit the harvested signaling molecules for estimation of the parameters of the channel, such as the degradation rate, viscosity, temperature, diffusion coefficient, is an interested topic for future research. Furthermore, investigating the impact of molecule harvesting on the energy efficiency of MC systems is also a promising research direction.

APPENDIX A
PROOF OF THEOREM 1

We denote the Fourier, inverse Fourier, Laplace, and inverse Laplace transforms by $F\{\cdot\}$, $F^{-1}\{\cdot\}$, $L\{\cdot\}$, and $L^{-1}\{\cdot\}$, respectively.

Let us start by solving (19) taking initial condition (20) into account. To this end, we take the Fourier transform of both (19) and (20) with respect to r' and solve the resulting equations. This leads to

$$U'(r', t'|r'_0) = \frac{\exp(-k'_{\rm d}t')}{8\pi r' r'_0 \sqrt{\pi t'}} \exp\left(\frac{-(r'-r'_0)^2}{4t'}\right). \quad (44)$$

In the next step, we solve (21) for initial condition (22). Here, by applying the Laplace transform with respect to t' to both (21) and (22) and then solving the resulting equations, we arrive at

$$\overline{V}(r', s|r'_0) = \frac{C}{r'} \exp\left(-r'\sqrt{s+k'_{\rm d}}\right), \quad (45)$$

where $\overline{V}(r', s|r'_0) = L\{V'(r', t'|r'_0)\}$, i.e.,

$$\overline{V}(r', s|r'_0) = \int_0^\infty V'\left(r', t'|r'_0\right) \exp(-st')\mathrm{d}t'. \quad (46)$$

In (45), C is a constant that can be used to ensure that $U'(r', t'|r'_0)$ and $V'(r', t'|r'_0)$ jointly satisfy boundary condition (17). We note that to obtain (45), we used the fact that $U'(r' \to \infty, t'|r'_0) = 0$ (see (44)). Thus, $V'(r' \to \infty, t'|r'_0) = 0$ in order to satisfy (9).

Now, in order to obtain C, one must calculate the Laplace transform of 1) $L\{P'_A(r', t'|r'_0)\} = \overline{P}_A(r', s|r'_0) = L\{U'(r', t'|r'_0)\} + L\{V'(r', t'|r'_0)\}$ and 2) boundary condition (17), and solve the resulting equations for C. Calculating $L\{U'(r', t'|r'_0)\}$ and using (45), we obtain

$$\overline{P}_A\left(r', s|r'_0\right) = \frac{\exp\left(-\sqrt{s+k'_{\rm d}}(r'-r'_0)\right)}{8\pi r' r'_0 \sqrt{s+k'_{\rm d}}} + \frac{C}{r'} \exp\left(-r'\sqrt{s+k'_{\rm d}}\right), \quad (47)$$

where we used [38, eq. (29.3.84)]

$$L\left\{\frac{1}{\sqrt{\pi t'}} \exp\left(\frac{-b^2}{4t'}\right)\right\} = \frac{\exp(-b\sqrt{s})}{\sqrt{s}} \quad (48)$$

for evaluation of $L\{U'(r', t'|r'_0)\}$. Taking the Laplace transform of (17) leads to

$$\left.\frac{\partial \overline{P}_A(r', s|r'_0)}{\partial r'}\right|_{r'=1} = \frac{k'_{\text{abs}}}{4\pi}\overline{P}_A(r', s|r'_0). \tag{49}$$

Solving (47) and (49) for C, and substituting the result back into (47), we arrive at

$$\begin{aligned} lCl\overline{P}_A(r', s|r'_0 = 1) = {} & \frac{\exp\left(-\sqrt{s+k'_{\text{d}}}(r'-1)\right)}{4\pi r'\sqrt{s+k'_{\text{d}}}} \\ & - \left[\frac{4\pi + k'_{\text{abs}}}{4\pi\sqrt{s+k'_{\text{d}}} + 4\pi + k'_{\text{abs}}}\right. \\ & \left. \times \frac{\exp\left(-\sqrt{s+k'_{\text{d}}}(r'-1)\right)}{4\pi r'\sqrt{s+k'_{\text{d}}}}\right]. \end{aligned} \tag{50}$$

Taking the inverse Laplace transform of (50) yields (23), where we used [38, eq. (29.3.90)]

$$\begin{aligned} L^{-1}\left\{\frac{\exp(-n\sqrt{s})}{\sqrt{s}(m+\sqrt{s})}\right\} = {} & \exp\left(nm + m^2 t'\right) \\ & \times \operatorname{erfc}\left(\frac{n}{2\sqrt{t'}} + m\sqrt{t}\right). \end{aligned} \tag{51}$$

APPENDIX B
PROOF OF THEOREM 2

Both $N'_{\text{on}}(t')$ and $N'_{\text{off}}(t')$ are the solution of the following integral with different integration limits

$$\Psi = \int P'_A(\tau'|r'_0)\mu'(t'-\tau')\mathrm{d}\tau'. \tag{52}$$

Thus, in the following, we solve (52). Using (28), we can write

$$\begin{aligned} \Psi &= \int \left((\mu'_0 + q't') - q'\tau'\right)P'_A(\tau'|r'_0)\mathrm{d}\tau' \\ &= \underbrace{\int (\mu'_0 + q't')P'_A(\tau'|r'_0)\mathrm{d}\tau'}_{\Psi_1} - \underbrace{\int q'\tau' P'_A(\tau'|r'_0)\mathrm{d}\tau'}_{\Psi_2}. \end{aligned} \tag{53}$$

We first solve Ψ_1. Given (25) and using integration by parts (i.e., $\int u\mathrm{d}v = uv - \int v\mathrm{d}u$) with $u = \exp(-k'_{\text{d}}\tau')$ and

$$\begin{aligned} \mathrm{d}v = {} & \frac{\varepsilon'}{\sqrt{\pi\tau'}}\exp\left(\frac{-\left(r'_{\text{rx}}-1\right)^2}{4\tau'}\right) + \varepsilon'\alpha'\exp\left(\alpha'\left(r'_{\text{rx}}-1\right)\right. \\ & \left. + (\alpha')^2\tau'\right)\operatorname{erfc}\left(\frac{r'_{\text{rx}}-1}{\sqrt{4\tau'}} + \alpha'\sqrt{\tau'}\right), \end{aligned} \tag{54}$$

Ψ_1 can be written as $\Psi_1 = (\mu'_0 + q't')[uv - \int v\mathrm{d}u]$. Let us first solve (54). For compactness, we define $\tilde{x}^2(\tau') = (r'_{\text{rx}}-1)^2/(4\tau')$, $\tilde{y}(\tau') = \alpha'(r'_{\text{rx}}-1) + (\alpha')^2\tau'$, and $\tilde{z}(\tau') = (r'_{\text{rx}}-1)/\sqrt{4\tau'} + \alpha'\sqrt{\tau'}$. Then, it is straightforward to show that $1/\sqrt{\pi\tau'} = 2/(\alpha'\sqrt{\pi})[\mathrm{d}\tilde{x}(\tau')/\mathrm{d}\tau' + \mathrm{d}\tilde{z}(\tau')/\mathrm{d}\tau']$. After taking the integral of both sides of (54), we have

$$\begin{aligned} v &= \varepsilon'\int \frac{2}{\alpha'\sqrt{\pi}}\left(\frac{\mathrm{d}\tilde{x}(\tau')}{\mathrm{d}\tau'} + \frac{\mathrm{d}\tilde{z}(\tau')}{\mathrm{d}\tau'}\right)\exp\left(-\tilde{x}^2(\tau')\right) \\ &\quad - \alpha'\exp\left(\tilde{y}(\tau')\right)\operatorname{erfc}\left(\tilde{z}(\tau')\right)\mathrm{d}\tau', \\ &= \frac{2\varepsilon'}{\alpha'\sqrt{\pi}}\int \frac{\mathrm{d}\tilde{x}(\tau')}{\mathrm{d}\tau'}\exp\left(-\tilde{x}^2(\tau')\right)\mathrm{d}\tau' \\ &\quad - \frac{\varepsilon'}{\alpha'}\int \frac{\mathrm{d}}{\mathrm{d}\tau'}\left(\exp\left(\tilde{y}(\tau')\right)\operatorname{erfc}\left(\tilde{z}(\tau')\right)\right)\mathrm{d}\tau', \\ &= \frac{\varepsilon'}{\alpha'}\left[\operatorname{erf}\left(\tilde{x}(\tau')\right) - \exp\left(\tilde{y}(\tau')\right)\operatorname{erfc}\left(\tilde{z}(\tau')\right)\right]. \end{aligned} \tag{55}$$

Considering (55) and $u = \exp(-k'_{\text{d}}\tau')$, $\Psi_{11} = uv$ can be obtained after back substituting $\tilde{x}(\tau')$, $\tilde{y}(\tau')$, and $\tilde{z}(\tau')$. Now, let us solve $\int v\mathrm{d}u$. Given (55) and $\mathrm{d}u = -k'_{\text{d}}\exp(-k'_{\text{d}}\tau')$, we can write

$$\begin{aligned} \int v\mathrm{d}u = \frac{-k'_{\text{d}}\varepsilon'}{\alpha'}\Bigg[& \underbrace{\int \operatorname{erf}\left(\frac{-(r'_{\text{rx}}-1)}{\sqrt{4\tau'}}\right)\exp\left(-k'_{\text{d}}\tau'\right)\mathrm{d}\tau'}_{\Psi_{12}} \\ & - \underbrace{\int \exp\left(\alpha'\left(r'_{\text{rx}}-1\right) + \left((\alpha')^2 - k'_{\text{d}}\right)\tau'\right)}_{\Psi_{13}} \\ & \times \underbrace{\operatorname{erfc}\left(\frac{r'_{\text{rx}}-1}{\sqrt{4\tau'}} + \alpha'\sqrt{\tau'}\right)\mathrm{d}\tau'}_{\Psi_{13}}\Bigg]. \end{aligned} \tag{56}$$

In (56), Ψ_{12} can be solved via (74) (in Appendix E) after substituting $\alpha' = 0$, $r' = r'_{\text{rx}}$, and $\operatorname{erfc}(\cdot) = 1 - \operatorname{erf}(\cdot)$. Moreover, the solution of integral Ψ_{13} is provided in Appendix F, and is obtained after substituting $x = \tau'$ and $r' = r'_{\text{rx}}$ in (77), shown at the bottom of the p. 18. Given Ψ_{11}, Ψ_{12}, and Ψ_{13}, Ψ_1 can be calculated as follows

$$\Psi_1 = \left(\mu'_0 + q't'\right)\left[\Psi_{11} + \left(\frac{k'_{\text{d}}\varepsilon'}{\alpha'}\right)[\Psi_{12} - \Psi_{13}]\right]. \tag{57}$$

This leads to (32).

Next, we calculate integral Ψ_2 in (53). In particular, Ψ_2 can be split into two integrals as follows

$$\begin{aligned} \Psi_2 = {} & q'\varepsilon'\underbrace{\int \frac{\tau'}{\sqrt{\pi\tau'}}\exp\left(\frac{-\left(r'_{\text{rx}}-1\right)^2}{4\tau'} - k'_{\text{d}}\tau'\right)\mathrm{d}\tau'}_{\Psi_{21}} \\ & + q'\varepsilon'\underbrace{\int -\alpha'\tau'\exp\left(\alpha'\left(r'-1\right) + (\alpha')^2\tau' - k'_{\text{d}}\tau'\right)}_{\Psi_{22}} \\ & \underbrace{\times \operatorname{erfc}\left(\frac{r'-1}{\sqrt{4\tau'}} + \alpha'\sqrt{\tau'}\right)\mathrm{d}\tau'}_{\Psi_{22}}. \end{aligned} \tag{58}$$

To solve Ψ_{21}, we use the change of variable $\sqrt{\tau'} = x$. Then, Ψ_{21} can be written in the form of (65), with the solution

given in (73) in Appendix D. This leads to the expression for Ψ_{21} given in (33). For deriving Ψ_{22}, let us define

$$f(\tau') = \exp\Big(\alpha'\big(r'-1\big) + (\alpha')^2\tau' - k'_{\rm d}\tau'\Big) \times \operatorname{erfc}\left(\frac{r'-1}{\sqrt{4\tau'}} + \alpha'\sqrt{\tau'}\right). \tag{59}$$

Then, employing integration by parts, we can write

$$\Psi_{22} = \tau' \int f(\tau')\mathrm{d}\tau' - \int \mathrm{d}\tau'\Big(\int f(\tau')\mathrm{d}\tau'\Big), \tag{60}$$

where $\int f(\tau')\mathrm{d}\tau'$ is solved via (77) in Appendix E after substituting x with τ', and $\int \mathrm{d}\tau'(\int f(\tau')\,\mathrm{d}\tau')$ is obtained by exploiting both (77) in Appendix E and (78) in Appendix E. The final expression for Ψ_{22} is given in (34).

APPENDIX C
PROOF OF THEOREM 3

Both $N'_{\rm Harv,on}(t')$ and $N'_{\rm Harv,off}(t')$ are the solution of $\Xi = \int P_A'^{\rm Harv}(\tau'|r'_0)\mu'(t'-\tau')\mathrm{d}\tau'$ with different limits of integration. Given (28), this integral can be split as follows

$$\Xi = \underbrace{\int \big(\mu'_0 + q't'\big)P_A'^{\rm Harv}(\tau'|r'_0)\mathrm{d}\tau'}_{\Xi_1} - q'\underbrace{\int \tau' P_A'^{\rm Harv}(\tau'|r'_0)\mathrm{d}\tau'}_{\Xi_2}. \tag{61}$$

Let us first evaluate Ξ_1. Given (26), we obtain

$$\Xi_1 = \frac{k'_{\rm abs}\big(\mu'_0 + q't'\big)}{4\pi} \times \Bigg[\underbrace{\int \frac{-\alpha'}{(\alpha')^2 - k'_{\rm d}}\exp\Big((\alpha')^2\tau' - k'_{\rm d}\tau'\Big)}_{\Xi_{11}}\underbrace{\times \operatorname{erfc}\big(\alpha'\sqrt{\tau}\big)\mathrm{d}\tau'}_{\Xi_{11}} + \underbrace{\int \frac{\sqrt{k'_{\rm d}}}{(\alpha')^2 - k'_{\rm d}}\operatorname{erfc}\left(\sqrt{k'_{\rm d}\tau'}\right)\mathrm{d}\tau'}_{\Xi_{12}} + \underbrace{\int \frac{1}{\alpha' + \sqrt{k'_{\rm d}}}\mathrm{d}\tau'}_{\Xi_{13}}\Bigg]. \tag{62}$$

In (62), Ξ_{11} can be solved via (77) (in Appendix E) after setting $r' = 1$. Ξ_{12} is obtained from (78) (in Appendix F) after setting $a = 0$ and $b = \sqrt{k'_{\rm d}}$. Furthermore, the solution of Ξ_{13} is equal to $\frac{\tau'}{\alpha' + \sqrt{k'_{\rm d}}}$. Eventually, this leads to (39).

Now, we evaluate Ξ_2. To do so, using (26), we arrive at

$$\Xi_2 = \frac{k'_{\rm abs}}{4\pi}\Bigg[\underbrace{\int \frac{-\alpha'\tau'}{(\alpha')^2 - k'_{\rm d}}\exp\Big((\alpha')^2\tau' - k'_{\rm d}\tau'\Big)}_{\Xi_{21}} \underbrace{\times \operatorname{erfc}\big(\alpha'\sqrt{\tau}\big)\mathrm{d}\tau'}_{\Xi_{21}} + \underbrace{\int \frac{\sqrt{k'_{\rm d}}}{(\alpha')^2 - k'_{\rm d}}\tau'\operatorname{erfc}\left(\sqrt{k'_{\rm d}\tau'}\right)\mathrm{d}\tau'}_{\Xi_{22}} + \underbrace{\int \frac{\tau'}{\alpha' + \sqrt{k'_{\rm d}}}\mathrm{d}\tau'}_{\Xi_{23}}\Bigg]. \tag{63}$$

In (63), evaluating Ξ_{21} requires the same steps as solving Ψ_{22} (in Appendix B) after setting $r' = 1$. For Ξ_{22}, after applying integration by parts twice, we obtain

$$\Xi_{22} = \frac{\sqrt{k'_{\rm d}}}{(\alpha')^2 - k'_{\rm d}}\Bigg[\frac{(\tau')^2}{2}\operatorname{erfc}\left(\sqrt{k'_{\rm d}\tau'}\right) + \frac{\sqrt{k'_{\rm d}}}{2\sqrt{\pi}}\Bigg(-\frac{1}{k'_{\rm d}} \times \exp\big(-k'_{\rm d}\tau'\big)(\tau')^{3/2} + \int \frac{3}{2k'_{\rm d}}\exp\big(-k'_{\rm d}\tau'\big)\sqrt{\tau'}\mathrm{d}\tau'\Bigg)\Bigg]. \tag{64}$$

The remaining integral in (64) is solved via (73) in Appendix D and setting $a = 0$ after performing the change of variable $\sqrt{\tau'} = x$. Moreover, the solution of Ξ_{23} is given by $\frac{(\tau')^2}{2(\alpha' + \sqrt{k'_{\rm d}})}$. Finally, combining the solutions of Ξ_{21}, Ξ_{22}, and Ξ_{23} in (64) leads to (40).

APPENDIX D

Here, we solve the following indefinite integral

$$\int x^2 \exp\Big(-\frac{a^2}{x^2} - bx^2\Big)\mathrm{d}x, \tag{65}$$

where a, b, and x are positive real numbers. To do so, we use the identity [39, eq. (5)]

$$\int \exp\Big(-\frac{a^2}{x^2} - bx^2\Big)\mathrm{d}x = \frac{\sqrt{\pi}}{4\sqrt{b}}\Big[e^{2a\sqrt{b}}\operatorname{erf}\Big(\frac{a}{x} + \sqrt{b}x\Big) - e^{-2a\sqrt{b}}\operatorname{erf}\Big(\frac{a}{x} - \sqrt{b}x\Big)\Big] + C \tag{66}$$

where C is a constant. By appropriately choosing C, and given that $\operatorname{erfc}(\cdot) = 1 - \operatorname{erf}(\cdot)$, (66) can be also written in the form of the complementary error function, i.e.,

$$\int \exp\Big(-\frac{a^2}{x^2} - bx^2\Big)\mathrm{d}x = \underbrace{\frac{\sqrt{\pi}}{4\sqrt{b}}\Big[e^{-2a\sqrt{b}}\operatorname{erfc}\Big(\frac{a}{x} - \sqrt{b}x\Big)}_{\gamma_1} \underbrace{- e^{2a\sqrt{b}}\operatorname{erfc}\Big(\frac{a}{x} + \sqrt{b}x\Big)\Big]}_{\gamma_1} + \tilde{C}, \tag{67}$$

where $\tilde{C}$ is the constant of integral. Eq. (67) is one of the key steps for solving (65). It is straightforward to see that taking the derivative (with respect to x) of the right-hand-side of (67) yields $\exp(-\frac{a^2}{x^2} - bx^2)$. Now, let us consider the right-hand-side of (67) after substituting the first $\operatorname{erfc}(\cdot)$-term with $1 + \operatorname{erf}(\cdot)$. Then, we have

$$\frac{\partial}{\partial x}\underbrace{\frac{\sqrt{\pi}}{4\sqrt{b}}\Big[e^{-2a\sqrt{b}}\Big(1 + \operatorname{erf}\Big(\frac{a}{x} - \sqrt{b}x\Big)\Big)}_{\gamma_2}$$

$$\underbrace{-\,e^{2a\sqrt{b}}\mathrm{erfc}\left(\frac{a}{x}+\sqrt{b}x\right)\Big]}_{\gamma_2}=-\frac{a}{\sqrt{b}x^2}e^{\left(-\frac{a^2}{x^2}-bx^2\right)}, \tag{68}$$

where we used

$$\frac{\partial \mathrm{erfc}\,(x)}{\partial x}=-\frac{2}{\sqrt{\pi}}\exp\Big(-x^2\Big), \tag{69}$$

$$\frac{\partial \mathrm{erf}\,(x)}{\partial x}=\frac{2}{\sqrt{\pi}}\exp\Big(-x^2\Big). \tag{70}$$

Furthermore, it is straightforward to show that

$$\frac{\partial}{\partial x}\underbrace{x\exp\left(-\frac{a^2}{x^2}-bx^2\right)}_{\gamma_3}=\exp\left(-\frac{a^2}{x^2}-bx^2\right)\times\left[1+\frac{2a^2}{x^2}-2bx^2\right]. \tag{71}$$

Now, using (67), (68), and (71), after some manipulations, we can write

$$\frac{\partial}{\partial x}\left[\frac{\gamma_1}{2b}-\frac{a\gamma_2}{\sqrt{b}}-\frac{\gamma_3}{2b}\right]=x^2\exp\left(-\frac{a^2}{x^2}-bx^2\right). \tag{72}$$

As a result, by integrating both sides of (72), we arrive at

$$\int x^2\exp\left(-\frac{a^2}{x^2}-bx^2\right)=\frac{\gamma_1}{2b}-\frac{a\gamma_2}{\sqrt{b}}-\frac{\gamma_3}{2b}+C. \tag{73}$$

APPENDIX E

In this Appendix, we solve the indefinite integral

$$\int f(x)\mathrm{d}x=\int\exp\Big(\Big((\alpha')^2-k_\mathrm{d}'\Big)x+\alpha'\big(r'-1\big)\Big)\times\mathrm{erfc}\left(\frac{r'-1}{\sqrt{4x}}+\alpha'\sqrt{x}\right)\mathrm{d}x. \tag{74}$$

For compactness, let us define $c=(\alpha')^2-k_\mathrm{d}'$ and $a=(r'-1)/\sqrt{4}$. Now, using integration by parts (i.e., $\int u\mathrm{d}v=uv-\int v\mathrm{d}u$) with $u=\mathrm{erfc}\,(\frac{a}{\sqrt{x}}+\alpha'\sqrt{x})$ and $e^{cx}\mathrm{d}x=\mathrm{d}v$, we can simplify (74) as follows

$$\int f(x)\mathrm{d}x=\frac{\exp\big(\alpha'\big(r'-1\big)\big)}{c}\Bigg[\exp(cx)\mathrm{erfc}\left(\frac{a}{\sqrt{x}}+\alpha'\sqrt{x}\right)+\underbrace{\int\frac{2}{\sqrt{\pi}}\exp\left(-\left(\frac{a}{\sqrt{x}}+\alpha'\sqrt{x}\right)^2+cx\right)\left(\frac{-a}{2x\sqrt{x}}+\frac{\alpha'}{2\sqrt{x}}\right)\mathrm{d}x}_{I}\Bigg]. \tag{75}$$

Using the substitution $\sqrt{x}=u$, I can be simplified as follows

$$I=\frac{-2}{\sqrt{\pi}}\int\exp\left(-\left(\frac{a}{u}+\alpha' u\right)^2+cu^2\right)\left(\frac{-a}{u^2}+\alpha'\right)\mathrm{d}u=\frac{-2e^{-2a\alpha'}}{\sqrt{\pi}}\left[\alpha'\underbrace{\int e^{-\left(\frac{a^2}{u^2}+k_\mathrm{d}'u^2\right)}\mathrm{d}u}_{I_1}-a\underbrace{\int\frac{1}{u^2}e^{-\left(\frac{a^2}{u^2}+k_\mathrm{d}'u^2\right)}\mathrm{d}u}_{I_2}\right]. \tag{76}$$

In (76), I_1 and I_2 can be solved using (67) and (68), respectively. Thus, exploiting (67), (68), and back substituting $u=\sqrt{x}$, the final expression is given by (77).

APPENDIX F

In this Appendix, we solve the indefinite integral

$$\int\mathrm{erfc}\left(\frac{a}{\sqrt{x}}+b\sqrt{x}\right)\mathrm{d}x, \tag{78}$$

where a and b are positive constants. Employing integration by parts (i.e., $\int u\mathrm{d}v=uv-\int v\mathrm{d}u$) with $u=\mathrm{erfc}\,(a/\sqrt{x}+b\sqrt{x})$ and $\mathrm{d}x=\mathrm{d}v$, we obtain

$$\int\mathrm{erfc}\left(\frac{a}{\sqrt{x}}+b\sqrt{x}\right)\mathrm{d}x=x\mathrm{erfc}\left(\frac{a}{\sqrt{x}}+b\sqrt{x}\right)-\underbrace{\int\frac{-2}{\sqrt{\pi}}e^{-\left(\frac{a}{\sqrt{x}}+b\sqrt{x}\right)^2}\left(\frac{-a}{2\sqrt{x}}+\frac{b\sqrt{x}}{2}\right)\mathrm{d}x}_{\Theta}. \tag{79}$$

Using the substitution $\sqrt{x}=u$, Θ can be simplified as follows

$$\Theta=\frac{-2e^{-2ab}}{\sqrt{\pi}}\left[b\underbrace{\int u^2e^{-\left(\frac{a^2}{u^2}+b^2u^2\right)}\mathrm{d}u}_{\Theta_1}-a\underbrace{\int e^{-\left(\frac{a^2}{u^2}+b^2u^2\right)}\mathrm{d}u}_{\Theta_2}\right]. \tag{80}$$

In (80), Θ_1 and Θ_2 can be solved by exploiting (73) and (67), respectively. As a result, the final solution is given in (81), shown at the bottom of the page.

$$\int f(x)\mathrm{d}x=\frac{-1}{2}\Bigg[\frac{\exp\Big(-\sqrt{k_\mathrm{d}'}(r'-1)\Big)}{\Big(\alpha'+\sqrt{k_\mathrm{d}'}\Big)\sqrt{k_\mathrm{d}'}}\mathrm{erf}\left(\frac{r'-1}{\sqrt{4x}}-\sqrt{k_\mathrm{d}'x}\right)+\frac{\exp\Big(-\sqrt{k_\mathrm{d}'}(r'-1)\Big)}{\Big(\alpha'-\sqrt{k_\mathrm{d}'}\Big)\sqrt{k_\mathrm{d}'}}\times\left(\exp\Big(2\sqrt{k_\mathrm{d}'}(r'-1)\Big)\mathrm{erfc}\left(\frac{r'-1}{\sqrt{4x}}+\sqrt{k_\mathrm{d}'x}\right)-1\right)-\frac{2}{\big((\alpha')^2-k_\mathrm{d}'\big)}\times\exp\Big(\Big((\alpha')^2-k_\mathrm{d}'\Big)x+\alpha'\big(r'-1\big)\Big)\mathrm{erfc}\left(\frac{r'-1}{\sqrt{4x}}+\alpha'\sqrt{x}\right)\Bigg]. \tag{77}$$

$$\int\mathrm{erfc}\left(\frac{a}{\sqrt{x}}+b\sqrt{x}\right)\mathrm{d}x=-\frac{e^{-4ab}}{4b^2}\left[\mathrm{erf}\left(\frac{a}{\sqrt{x}}-b\sqrt{x}\right)+(4ab-1)\left(e^{4ab}\mathrm{erf}\left(\frac{a}{\sqrt{x}}+b\sqrt{x}\right)-e^{4ab}+1\right)\right]+x\mathrm{erfc}\left(\frac{a}{\sqrt{x}}+b\sqrt{x}\right)+\frac{1}{b\sqrt{\pi}}x\exp\left(-\frac{(a+bx)^2}{x}\right). \tag{81}$$

REFERENCES

[1] I. F. Akyildiz, F. Brunetti, and C. Blázquez, "Nanonetworks: A new communication paradigm," *Comput. Netw.*, vol. 52, no. 12, pp. 2260–2279, Aug. 2008.

[2] T. Nakano, A. W. Eckford, and T. Haraguchi, *Molecular Communication*. Cambridge, U.K.: Cambridge Univ. Press, 2013.

[3] N. Farsad, H. B. Yilmaz, A. Eckford, C.-B. Chae, and W. Guo, "A comprehensive survey of recent advancements in molecular communication," *IEEE Commun. Surveys Tuts.*, vol. 18, no. 3, pp. 1887–1919, 3rd Quart., 2016.

[4] V. Jamali, A. Ahmadzadeh, W. Wicke, A. Noel, and R. Schober, "Channel modeling for diffusive molecular communication—A tutorial review," *Proc. IEEE*, vol. 107, no. 7, pp. 1256–1301, Jul. 2019.

[5] B. Alberts *et al.*, *Essential Cell Biology*, 3rd ed. New York, NY, USA: Garland Sci., 2009.

[6] S. T. Brady, G. J. Siegel, R. W. Albers, and D. L. Price, *Basic Neurochemistry: Principles of Molecular, Cellular, and Medical Neurobiology*. Amsterdam, The Netherlands: Elsevier, 2012.

[7] Y. Tang, M. Wen, X. Chen, Y. Huang, and L.-L. Yang, "Molecular type permutation shift keying for molecular communication," *IEEE Trans. Mol. Biol. Multi-Scale Commun.*, vol. 6, no. 2, pp. 160–164, Nov. 2020.

[8] M. C. Gursoy, D. Seo, and U. Mitra, "A concentration-time hybrid modulation scheme for molecular communications," *IEEE Trans. Mol. Biol. Multi-Scale Commun.*, vol. 7, no. 4, pp. 288–299, Dec. 2021.

[9] B. Dhayabaran, G. T. Raja, and M. Magarini, "Low complex receiver design for modified inverse source coded diffusion-based molecular communication systems," *IEEE Trans. Mol. Biol. Multi-Scale Commun.*, vol. 7, no. 4, pp. 239–252, Dec. 2021.

[10] J. W. Kwak, H. B. Yilmaz, N. Farsad, C.-B. Chae, and A. J. Goldsmith, "Two-way molecular communications," *IEEE Trans. Commun.*, vol. 68, no. 6, pp. 3550–3563, Jun. 2020.

[11] M. Farahnak-Ghazani, G. Aminian, M. Mirmohseni, A. Gohari, and M. Nasiri-Kenari, "On medium chemical reaction in diffusion-based molecular communication: A two-way relaying example," *IEEE Trans. Commun.*, vol. 67, no. 2, pp. 1117–1132, Feb. 2019.

[12] L. Khaloopour, M. Mirmohseni, and M. Nasiri-Kenari, "Adaptive release duration modulation for limited molecule production and storage," *IEEE Trans. Mol. Biol. Multi-Scale Commun.*, vol. 5, no. 2, pp. 139–152, Nov. 2019.

[13] B. Dhayabaran, G. T. Raja, M. Magarini, and H. B. Yilmaz, "Transmit signal shaping for molecular communication," *IEEE Wireless Commun. Lett.*, vol. 10, no. 7, pp. 1459–1463, Jul. 2021.

[14] A. Noel, D. Makrakis, and A. Hafid, "Channel impulse responses in diffusive molecular communication with spherical transmitters," in *Proc. Biennial Symp. Commun.*, Apr. 2016, p. 6. [Online]. Available: http://arxiv.org/abs/1604.04684

[15] H. B. Yilmaz, G.-Y. Suk, and C.-B. Chae, "Chemical propagation pattern for molecular communications," *IEEE Wireless Commun. Lett.*, vol. 6, no. 2, pp. 226–229, Apr. 2017.

[16] H. Arjmandi, A. Ahmadzadeh, R. Schober, and M. N. Kenari, "Ion channel based bio-synthetic modulator for diffusive molecular communication," *IEEE Trans. NanoBiosci.*, vol. 15, no. 5, pp. 418–432, Jul. 2016.

[17] C. T. Chou, "A Markovian approach to the optimal demodulation of diffusion-based molecular communication networks," *IEEE Trans. Commun.*, vol. 63, no. 10, pp. 3728–3743, Oct. 2015.

[18] H. Awan and C. T. Chou, "Generalized solution for the demodulation of reaction shift keying signals in molecular communication networks," *IEEE Trans. Commun.*, vol. 65, no. 2, pp. 715–727, Feb. 2017.

[19] H. Awan and C. T. Chou, "Molecular circuit-based transmitters and receivers for molecular communication networks," in *Proc. IEEE Int. Workshop Signal Process. Adv. Wireless Commun. (SPAWC)*, Sapporo, Japan, Jul. 2017, pp. 1–5.

[20] X. Huang, Y. Fang, A. Noel, and N. Yang, "Membrane fusion-based transmitter design for static and diffusive mobile molecular communication systems," 2021, *arXiv:2104.11864*.

[21] W. Guo *et al.*, "SMIET: Simultaneous molecular information and energy transfer," *IEEE Wireless Commun.*, vol. 25, no. 1, pp. 106–113, Feb. 2018.

[22] Y. Deng, W. Guo, A. Noel, A. Nallanathan, and M. Elkashlan, "Enabling energy efficient molecular communication via molecule energy transfer," *IEEE Commun. Lett.*, vol. 21, no. 2, pp. 254–257, Feb. 2017.

[23] S. Lotter, A. Ahmadzadeh, and R. Schober, "Synaptic channel modeling for DMC: Neurotransmitter uptake and spillover in the tripartite synapse," *IEEE Trans. Commun.*, vol. 69, no. 3, pp. 1462–1479, Mar. 2021.

[24] L. Grebenstein *et al.*, "Biological optical-to-chemical signal conversion interface: A small-scale modulator for molecular communications," *IEEE Trans. NanoBiosci.*, vol. 18, no. 1, pp. 31–42, Jan. 2019.

[25] C. A. Söldner *et al.*, "A survey of biological building blocks for synthetic molecular communication systems," *IEEE Commun. Surveys Tuts.*, vol. 22, no. 4, pp. 2765–2800, 4th Quart., 2020.

[26] S. Y. Shvartsman, H. S. Wiley, W. M. Deen, and D. A. Lauffenburger, "Spatial range of autocrine signaling: Modeling and computational analysis," *Biophys. J.*, vol. 81, no. 4, pp. 1854–1867, Oct. 2001.

[27] S. S. Andrews and D. Bray, "Stochastic simulation of chemical reactions with spatial resolution and single molecule detail," *Phys. Biol.*, vol. 1, nos. 3–4, pp. 137–151, Dec. 2004.

[28] A. Noel, K. C. Cheung, and R. Schober, "Improving receiver performance of diffusive molecular communication with enzymes," *IEEE Trans. NanoBiosci.*, vol. 13, no. 1, pp. 31–43, Mar. 2014.

[29] C. T. Chou, "Noise properties of linear molecular communication networks," *Nano Commun. Netw.*, vol. 4, no. 3, pp. 87–97, 2013.

[30] A. Ahmadzadeh, H. Arjmandi, A. Burkovski, and R. Schober, "Comprehensive reactive receiver modeling for diffusive molecular communication systems: Reversible binding, molecule degradation, and finite number of receptors," *IEEE Trans. NanoBiosci.*, vol. 15, no. 7, pp. 713–727, Oct. 2016.

[31] D. T. Gillespie and E. Seitaridou, *Simple Brownian Diffusion: An Introduction to the Standard Theoretical Models*. Oxford, U.K.: Oxford Univ. Press, 2013.

[32] P. Grindrod, *The Theory and Applications of Reaction-Diffusion Equations: Patterns and Waves*. Oxford, U.K.: Clarendon Press, 1996.

[33] H. Kim and K. J. Shin, "Exact solution of the reversible diffusion-influenced reaction for an isolated pair in three dimensions," *Phys. Rev. Lett.*, vol. 82, pp. 1578–1581, Feb. 1999.

[34] I. Stakgold and M. J. Holst, *Green's Functions and Boundary Value Problems*. Hoboken, NJ, USA: Wiley, 2011.

[35] K. Schulten and I. Kosztin, *Lectures in Theoretical Biophysics*. Champaign, IL, USA: Univ. Illinois Urbana-Champaign, 2000.

[36] R. Khanin, H. Parnas, and L. Segel, "Diffusion cannot govern the discharge of neurotransmitter in fast synapses," *Biophys. J.*, vol. 67, no. 3, pp. 966–972, Sep. 1994.

[37] A. Noel, K. C. Cheung, and R. Schober, "Joint channel parameter estimation via diffusive molecular communication," *IEEE Trans. Mol. Biol. Multi-Scale Commun.*, vol. 1, no. 1, pp. 4–17, Mar. 2015.

[38] M. Abramowitz and I. Stegun, *Handbook of Mathematical Functions*, 1st ed. New York, NY, USA: Dover, 1964.

[39] E. W. Ng and M. Geller, "A table of integrals of the error functions," *J. Res. Nat. Bureau Stand. B, Math. Sci.*, vol. 73B, no. 1, pp. 1–20, Jan.–Mar. 1969.

ARMAN AHMADZADEH received the B.Sc. degree in electrical engineering from the Ferdowsi University of Mashhad, Mashhad, Iran, in 2010, and the M.Sc. degree in communications and multimedia engineering from Friedrich-Alexander University, Erlangen, Germany, in 2013, where he currently pursuing the Ph.D. degree in electrical engineering with the Institute for Digital Communications. Since 2019, he has been joined Fraunhofer Institute for Integrated Circuits, where he is currently working as Radio Access Network Working Group 1 3GPP delegate on radio layer 1 specifications of 5G New Radio standard. His research interests include wireless communications and molecular communications. He received several awards, including the Best Paper Award from the IEEE International Conference on Communications (ICC) in 2016 and the IEEE ICC in 2020, the Student Travel Grants for attending the IEEE Global Communications Conference (GLOBECOM) in 2017, and the Best Journal Paper Award (Literaturpreis) from the German Information Technology Society (ITG) in 2020. He served as a member of Technical Program Committees of the Communication Theory Symposium for the IEEE ICC from 2017 to 2020 and the Selected Areas in Communications Symposium for the IEEE GLOBECOM from 2020 to 2022. He was recognized as an Exemplary Reviewer of the IEEE COMMUNICATIONS LETTERS in 2016.

VAHID JAMALI (Member, IEEE) received the B.Sc. and M.Sc. degrees (Hons.) in electrical engineering from the K. N. Toosi University of Technology, Tehran, Iran, in 2010 and 2012, respectively, and the Ph.D. degree (Hons.) from the Friedrich-Alexander-University (FAU) of Erlangen–Nürnberg, Erlangen, Germany, in 2019. In 2017, he was a Visiting Research Scholar with Stanford University, Stanford, CA, USA. He is currently a Postdoctoral Research Fellow with the Department of Electrical and Computer Engineering, Princeton University. His research interests include wireless and molecular communications and multiuser information theory. He has received several awards for his publications and research work, including the Best Paper Awards from the IEEE ICC in 2016, the ACM NanoCOM in 2019, the Asilomar CSSC in 2020, and the IEEE WCNC in 2021; the Doctoral Research Grant from the German Academic Exchange Service (DAAD) in 2017; the Best Ph.D. Thesis Presentation Award from the IEEE WCNC in 2018; the Best Journal Paper Award (Literaturpreis) from the German Information Technology Society (ITG) in 2020; and the Postdoctoral Research Fellowship by the German Research Foundation (DFG) in 2020. He is an Associate Editor of the IEEE COMMUNICATIONS LETTERS, IEEE OPEN JOURNAL OF THE COMMUNICATIONS SOCIETY, and *Physical Communication* (Elsevier). He has served as a member of the technical program committee for several IEEE conferences.

ROBERT SCHOBER (Fellow, IEEE) received the Diploma (Univ.) and Ph.D. degrees in electrical engineering from the Friedrich-Alexander University of Erlangen–Nuremberg (FAU), Germany, in 1997 and 2000, respectively. From 2002 to 2011, he was a Professor and a Canada Research Chair with The University of British Columbia (UBC), Vancouver, BC, Canada. Since January 2012, he has been an Alexander von Humboldt Professor and the Chair of Digital Communication with FAU. His research interests fall into the broad areas of communication theory, wireless communications, and statistical signal processing. He has received several awards for his work, including the 2002 Heinz Maier-Leibnitz Award of the German Science Foundation (DFG), the 2004 Innovations Award of the Vodafone Foundation for Research in Mobile Communications, the 2006 UBC Killam Research Prize, the 2007 Wilhelm Friedrich Bessel Research Award of the Alexander von Humboldt Foundation, the 2008 Charles McDowell Award for Excellence in Research from UBC, the 2011 Alexander von Humboldt Professorship, the 2012 NSERC E. W. R. Stacie Fellowship, and the 2017 Wireless Communications Recognition Award by the IEEE WIRELESS COMMUNICATIONS Technical Committee. Since 2017, he has been listed as a Highly Cited Researcher by the Web of Science. From 2012 to 2015, he served as the Editor-in-Chief for the IEEE TRANSACTIONS ON COMMUNICATIONS. He currently serves as a member of the Editorial Board for the PROCEEDINGS OF THE IEEE and a VP for the Publications of the IEEE Communication Society. He is a Fellow of the Canadian Academy of Engineering and the Engineering Institute of Canada.